1. Introduction

It was observed by 't Hooft [1] that the standard model does not conserve baryon and lepton number due to Adler-Bell-Jackiw anomalies [2]. The process 't Hooft [1] considered was fermion number violation due to instanton induced transitions. Attracting much attention [3] Ringwald [4] recently argued, that such tunnelling transitions between topologically distinct vacua might indeed be observable in future accelerators.

The possibility of baryon and lepton number violation in the standard model was considered from another point of view by Manton [5]. Investigating the topology in the Weinberg-Salam theory, Manton showed that there are noncontractible loops in configuration space, and predicted the existence of a static, unstable solution of the field equations, a sphaleron [6], which would represent the top of the energy barrier between topologically distinct vacua.

Since at finite temperature this energy barrier between topologically distinct vacua can be overcome due to thermal fluctuations of the fields, baryon number violating vacuum to vacuum transitions can occur. The rate for such baryon number violating processes is largely determined by a Boltzmann factor, containing the height of the barrier at a given temperature and thus the energy of the sphaleron [7-10]. Baryon number violation in the standard model due to such transitions over the barrier may be relevant for the physics of the early universe, necessitating new scenarios for the generation of the baryon asymmetry [7-10].

In the limit of vanishing mixing angle $\theta_w = 0$ the electroweak sphaleron is well known [6,11]. In this limit the U(1) field decouples, and the energy density of the SU(2) sphaleron has spherical symmetry. At finite mixing angle the coupling to the U(1) field destroys the spherical symmetry, and the sphaleron retains only axial symmetry [6,12]. Here we consider the sphaleron of the full Weinberg-Salam theory, treating the mixing angle θ_w as a parameter, which is varied over the range $0 \leq \theta_w \leq \pi/2$.

The appropriate ansatz [12] for the axially symmetric sphaleron is analogous to the one for multimonopoles [13]. In both cases there is an abelian gauge transformation, which preserves the structure of the ansatz [12,13]. Thus for the construction of the sphaleron a gauge fixing condition must be chosen. In the limit $\theta_w = 0$ the sphaleron is symmetric under parity reflections. Therefore we also require parity reflection symmetry for the sphaleron at finite mixing angle [12]. (We do not consider here the 'deformed' sphalerons, which appear for large Higgs masses and which break this symmetry [14,15].)

In section 2 we present the ansatz and the energy functional. Further we discuss the residual abelian gauge invariance and several choices of gauge. Due to the axial symmetry of the sphaleron at finite mixing angle, the unknown gauge and Higgs field functions entering in the ansatz, depend on two variables. They represent the dynamical degrees of freedom of the system. In section 3 we expand these functions in terms of Legendre polynomials [16,17] and solve the resulting system of coupled *ordinary* differential equations numerically. We perform the expansion up to sixth order terms and consider the convergence of the series as a function of the weak mixing angle. We discuss the results obtained in several gauges. In section 4 we solve the full system of

coupled *partial* differential equations numerically and compare with the results of the expansion. We give our conclusions in section 5.

2. Ansatz and energy density

Let us consider the bosonic sector of the Weinberg-Salam theory. It has the lagrangian density

$$L = -\frac{1}{4}F^a_{\mu\nu}F^{a\mu\nu} - \frac{1}{4}f_{\mu\nu}f^{\mu\nu} + (D_\mu\Phi)^\dagger(D^\mu\Phi) - \lambda(\Phi^\dagger\Phi - \frac{v^2}{2})^2 \qquad (2.1)$$

with the usual definitions for the SU(2) field strength tensor $F^a_{\mu\nu}$, the U(1) field strength tensor $f_{\mu\nu}$ and the covariant derivative for the Higgs field $D_\mu\Phi$.

The gauge symmetry is spontaneously broken via the Higgs potential, leading to a nonvanishing expectation value for the Higgs field

$$\langle\Phi\rangle = \frac{v}{\sqrt{2}}\begin{pmatrix}0\\1\end{pmatrix} \qquad (2.2)$$

and the masses of gauge and Higgs bosons

$$M_W = \frac{1}{2}gv \quad , \quad M_Z = \frac{1}{2}\sqrt{(g^2+g'^2)}v \quad , \quad M_H = v\sqrt{2\lambda}\,. \qquad (2.3)$$

The mixing angle θ_w is determined by the relation $\tan\theta_w = g'/g$, and the electric charge is $e = g\sin\theta_w$.

2.1 Ansatz for the axially symmetric sphaleron

Let us now consider the ansatz for the fields. Due to the coupling to the U(1) field, for finite values of the mixing angle θ_w we can require only axial symmetry around the z-axis for the electroweak sphaleron. The appropriate ansatz for the fields [12] is analogous to the one discussed by Manton[13] and Rebbi and Rossi [16] for axially symmetric multimonopoles.

We define a set of orthonormal vectors

$$\begin{aligned}\vec{u}_1(\phi) &= (\cos\phi, \sin\phi, 0)\\ \vec{u}_2(\phi) &= (0,0,1)\\ \vec{u}_3(\phi) &= (\sin\phi, -\cos\phi, 0)\ ,\end{aligned} \qquad (2.4)$$

and expand the fields as follows

$$W^a_i(\vec{r}) = u^i_j(\phi)u^a_k(\phi)w^k_j(\rho,z)\ , \qquad (2.5a)$$

$$A_i(\vec{r}) = u^i_j(\phi)a_j(\rho,z)\ , \qquad (2.5b)$$

$$\Phi(\vec{r}) = i r^i u^i_j(\phi) h_j(\rho,z) \frac{v}{\sqrt{2}} \begin{pmatrix} 0 \\ 1 \end{pmatrix} . \qquad (2.5c)$$

To incorporate invariance under rotations around the z-axis we choose for the SU(2) field and the Higgs field the conditions

$$w^1_1(\rho,z) = w^1_2(\rho,z) = w^2_1(\rho,z) = w^2_2(\rho,z) = w^3_3(\rho,z) = 0 , \qquad (2.6a)$$

$$h_3(\rho,z) = 0 , \qquad (2.6b)$$

and for the U(1) field

$$a_1(\rho,z) = a_2(\rho,z) = 0 . \qquad (2.6c)$$

2.2 Axially symmetric energy density

The resulting energy functional E is axially symmetric

$$E = \frac{1}{2} \int (E_w + E_a + v^2 E_h)\, d\phi\, \rho d\rho\, dz \qquad (2.7a)$$

and has the contributions

$$\begin{aligned} E_w = &(\partial_\rho w^1_3 + \frac{1}{\rho}(w^3_1 + w^1_3) - g w^3_1 w^2_3)^2 + (\partial_z w^1_3 + \frac{1}{\rho} w^3_2 - g w^3_2 w^2_3)^2 \\ &+ (\partial_\rho w^2_3 + \frac{1}{\rho} w^2_3 + g w^3_1 w^1_3)^2 + (\partial_z w^2_3 + g w^3_2 w^1_3)^2 + (\partial_\rho w^3_2 - \partial_z w^3_1)^2 , \end{aligned} \qquad (2.7b)$$

$$E_a = (\partial_\rho a_3 + \frac{1}{\rho} a_3)^2 + (\partial_z a_3)^2 , \qquad (2.7c)$$

$$\begin{aligned} E_h = &(\partial_\rho h_1 - \frac{g}{2} w^3_1 h_2)^2 + (\partial_z h_1 - \frac{g}{2} w^3_2 h_2)^2 + (\partial_\rho h_2 + \frac{g}{2} w^3_1 h_1)^2 + (\partial_z h_2 + \frac{g}{2} w^3_2 h_1)^2 \\ &+ (\frac{1}{\rho} h_1 + \frac{g}{2}(w^1_3 h_2 - w^2_3 h_1) - \frac{g'}{2} a_3 h_1)^2 + (\frac{g}{2}(w^1_3 h_1 + w^2_3 h_2) - \frac{g'}{2} a_3 h_2)^2 \\ &+ \frac{\lambda v^2}{2}(h^2_1 + h^2_2 - 1)^2 . \end{aligned} \qquad (2.7d)$$

2.3 Residual U(1) gauge invariance

The energy functional eq.(2.7) is still invariant under gauge transformations generated by

$$U = e^{i\Gamma(\rho,z) \tau^i u^i_3} , \qquad (2.8)$$

again analogous to the energy density of multimonopoles [13,16]. Under such a gauge transformation the 2-D Higgs doublets (h_1, h_2) and $(w^1_3, w^2_3 - 1/g\rho)$ transform with angle $\Gamma(\rho,z)$ and $2\Gamma(\rho,z)$, respectively, while the 2-D gauge field (w^3_1, w^3_2) transforms inhomogeneously.

In order to construct the sphaleron solution, we have to fix a gauge. This appears to be a rather subtle problem.

a) 'Coulomb gauge'

We will present most of our results for the sphaleron in the following gauge, to which we will refer as 'Coulomb gauge'. We fix the gauge degree of freedom by choosing the gauge condition

$$G_{gf} = \partial_\rho w_1^3 + \partial_z w_2^3 = 0 \ . \tag{2.9}$$

This gauge is implemented by adding the term

$$\frac{\xi}{2} \int (G_{gf})^2 \, d\phi \, \rho d\rho \, dz \tag{2.10}$$

to the energy functional with $\xi = 1$.

b) 'Hedgehog gauge'

Another gauge we consider, we will refer to as 'hedgehog gauge', since the Higgs field assumes the 'hedgehog' form

$$\Phi'(\vec{r}) = U_h \Phi(\vec{r}) = i\tau^i \hat{r}^i L(\rho, z) \frac{v}{\sqrt{2}} \begin{pmatrix} 0 \\ 1 \end{pmatrix} \ , \tag{2.11}$$

where $\hat{r}$ denotes the unit vector. In this gauge the Higgs field is described by only one unknown function $L(\rho, z)$. Starting from a regular sphaleron solution with the Higgs field

$$\Phi(\vec{r}) = i(\tau^i u_1^i h_1(\rho, z) + \tau^i u_2^i h_2(\rho, z)) \frac{v}{\sqrt{2}} \begin{pmatrix} 0 \\ 1 \end{pmatrix}$$

the gauge transformation U_h to the 'hedgehog gauge' involves the function $\Gamma_h(\rho, z)$, determined via

$$\tan \Gamma_h(\rho, z) = \frac{-z h_1(\rho, z) + \rho h_2(\rho, z)}{\rho h_1(\rho, z) + z h_2(\rho, z)} \ . \tag{2.12}$$

c) 'Physical gauge'

We also consider the 'physical gauge', where the Higgs field assumes its vacuum expectation value asymptotically. In this gauge the Higgs field assumes the form

$$\Phi'(\vec{r}) = L(\rho, z) \frac{v}{\sqrt{2}} \begin{pmatrix} 0 \\ 1 \end{pmatrix} \ . \tag{2.13}$$

It is obtained from the 'hedgehog gauge' by the further transformation

$$U_p = e^{i(\pi/2)\tau^i \hat{r}^i} = i\tau^i \hat{r}^i \ . \tag{2.14}$$

While E_w remains form invariant under this transformation, E_h changes to

$$\begin{aligned} E_h = & (\partial_\rho L)^2 + (\partial_z L)^2 \\ & + L^2 (\frac{g}{2})^2 ((w'^3_1)^2 + (w'^3_2)^2 + (w'^1_3)^2) + L^2 (\frac{g}{2} w'^2_3 - \frac{g'}{2} a_3)^2 \\ & + \frac{\lambda v^2}{2} (L^2 - 1)^2 \ . \end{aligned} \tag{2.15}$$

2.4 Ansatz with parity reflection symmetry

By requiring parity reflection symmetry now in addition to axial symmetry, we can specify the ansatz eqs.(2.5)-(2.6) further [12,16]. Changing to spherical coordinates, we define the functions $F_i(r,\theta)$

$$\begin{aligned} w_1^3(r,\theta) &= \frac{2}{gr}F_1(r,\theta)\cos\theta\ , \quad & w_2^3(r,\theta) &= -\frac{2}{gr}F_2(r,\theta)\sin\theta\ , \\ w_3^1(r,\theta) &= -\frac{2}{gr}F_3(r,\theta)\cos\theta\ , \quad & w_3^2(r,\theta) &= \frac{2}{gr}F_4(r,\theta)\sin\theta\ , \end{aligned} \tag{2.16a}$$

$$h_1(r,\theta) = F_5(r,\theta)\sin\theta\ , \quad h_2(r,\theta) = F_6(r,\theta)\cos\theta\ , \tag{2.16b}$$

and

$$a_3(r,\theta) = \frac{2}{g'r}F_7(r,\theta)\sin\theta\ . \tag{2.16c}$$

With these functions $F_i(r,\theta)$ the spherically symmetric ansatz, valid in the limit $g' \to 0$, is recovered, when

$$F_1(r,\theta) = F_2(r,\theta) = F_3(r,\theta) = F_4(r,\theta) = f(r)\ ,$$

$$F_5(r,\theta) = F_6(r,\theta) = h(r)$$

and

$$F_7(r,\theta) = 0\ ,$$

where the functions $f(r)$ and $h(r)$ correspond to those of ref. [6].

2.5 Boundary conditions

a) 'Coulomb gauge'

To obtain regular, finite energy solutions with the imposed symmetries, we choose as boundary conditions for the functions $F_i(r,\theta)$ in the 'Coulomb gauge' [12]

$$\begin{aligned} r = 0:&\ F_i(r,\theta)|_{r=0} = 0, && i = 1,...,7 \\ r \to \infty:&\ F_i(r,\theta)|_{r=\infty} = 1, && i = 1,...,6, \quad F_7(r,\theta)|_{r=\infty} = 0 \\ \theta = 0:&\ \partial_\theta F_i(r,\theta)|_{\theta=0} = 0, && i = 1,...,7 \\ \theta = \pi/2:&\ \partial_\theta F_i(r,\theta)|_{\theta=\pi/2} = 0, && i = 1,...,7\ . \end{aligned} \tag{2.17}$$

In the 'Coulomb gauge' we must then solve for all seven functions $F_i(r,\theta)$. Inspection of the energy density eq.(2.7d) yields for the long-ranged functions $F_3(r,\theta)$, $F_4(r,\theta)$ and $F_7(r,\theta)$ the asymptotic relations

$$\begin{aligned} F_3(r,\theta) &\to 1 - 2\sin^2\theta\, F_7(r,\theta)\ , \\ F_4(r,\theta) &\to 1 - (2\sin^2\theta - 1)\, F_7(r,\theta)\ . \end{aligned} \tag{2.18}$$

b) 'Hedgehog gauge'

In the 'hedgehog gauge' we have to solve for only six functions, since

$$F_5(r,\theta) = F_6(r,\theta) = L(r,\theta) \ . \tag{2.19}$$

Taking eq.(2.19) into account, the boundary conditions are the same as in eq.(2.17). The 'hedgehog gauge' was used by Rebbi and Rossi [16] for the construction of multimonopoles.

c) 'Physical gauge'

In the 'physical gauge' the SU(2) gauge field functions $F_i(r,\theta)$, $i = 1,...,4$, change according to

$$\begin{aligned} &F_i(r,\theta) \to 1 - F_i(r,\theta), \quad i = 1,2 \ , \\ &F_3(r,\theta) \to 1 - F_3(r,\theta) + 2\sin^2\theta(F_3(r,\theta) - F_4(r,\theta)) \ , \\ &F_4(r,\theta) \to 1 - F_4(r,\theta) - 2\cos^2\theta(F_3(r,\theta) - F_4(r,\theta)) \end{aligned} \tag{2.20}$$

with respect to the 'hedgehog gauge', while the Higgs field function $L(r,\theta)$ remains unchanged. Here only the functions $F_4(r,\theta)$ and $F_7(r,\theta)$ are long-ranged with the asymptotic relation

$$F_4(r,\theta) \to F_7(r,\theta) \ . \tag{2.21}$$

2.6 Parameters

With the appropriate boundary conditions we solve numerically for the functions $F_i(r,\theta)$, using dimensionless coordinates $x = gvr$. We fix the parameters $g = 0.65$ and $M_W = 80\text{GeV}$. We vary the Higgs mass, though most calculations are performed for $M_H = M_W$; and we vary the mixing angle between $0 \leq \theta_w \leq \pi/2$, with physical value $\theta_w = 0.5$.

3. Results: Legendre polynomial expansion

To construct the sphaleron at finite mixing angle θ_w in general we have to solve a system of coupled non-linear *partial* differential equations. Since this is a demanding numerical task, we will first discuss an approximate method of solution: We expand the functions $F_i(x,\theta)$, depending on two variables, in terms of Legendre polynomials $P_l(\cos\theta)$. By minimizing the energy functional we then obtain a system of coupled non-linear *ordinary* differential equations for the unknown coefficient functions $f_{i,l}(x)$, which is solved numerically.

Such an expansion in terms of Legendre polynomials was applied by Rebbi and Rossi [16] for the construction of multimonopoles. But instead of solving differential equations for the functions $f_{i,l}(x)$, they introduced an additional expansion for the functions $f_{i,l}(x)$ and then minimized the energy functional with respect to the resulting sets of constant coefficients.

Due to the parity reflection symmetry of the sphaleron only even Legendre polynomials contribute in the expansion [16], i.e. $l = 0, 2, 4, 6...$. In the following we will first discuss the 0th order expansion, and then the higher order expansions, presenting results up to the 6th order.

3.1 0th order Legendre polynomial expansion

In the limit of vanishing mixing angle, the sphaleron is spherical. Therefore an expansion in Legendre polynomials would have only non-vanishing lowest order terms

$$F_i(x,\theta) = f_{i,0}(x) P_0(\cos\theta) = f_{i,0}(x) \ . \tag{3.1}$$

For small but finite mixing angles, we expect, that the 0th order expansion will do quite well, while for larger mixing angles higher order terms should become increasingly important.

Requiring a finite energy density and a finite energy leads to a restriction on the 0th order functions $f_{i,0}(x)$. The SU(2) gauge part of the energy density eq.(2.7b) contains in its first term the expression

$$\frac{1}{\rho}(w_1^3 + w_3^1) = \frac{2gv^2}{x^2}(F_1(x,\theta) - F_3(x,\theta))\frac{\cos\theta}{\sin\theta} \ , \tag{3.2a}$$

which implies a singular behaviour along the z-axis unless

$$F_1(x, \theta = 0) = F_3(x, \theta = 0) \ . \tag{3.2b}$$

Since in 0th order the functions $F_i(x,\theta)$ do not depend on θ, we must require

$$f_{1,0}(x) = f_{3,0}(x) \tag{3.2c}$$

to avoid the singular behaviour. This leaves one independent function $f_{i,0}(x)$ less to be determined.

In the following we consider the 0th order expansion in the 'Coulomb gauge' and in the 'physical gauge', and the further restricted expansion of ref. [17].

a) 'Coulomb gauge'

Due to the restriction (3.2c) in the 'Coulomb gauge' six independent functions $f_{i,0}(x)$ ought be determined. Inspection of the asymptotic relations (2.18), however, shows, that this gauge is inadequate, when only 0th order terms are taken into account. These relations clearly require an asymptotic θ-dependence for the functions $F_3(x,\theta)$ and $F_4(x,\theta)$, if $F_7(x,\theta)$ is long-ranged, even if $F_7(x,\theta)$ were independent of θ. Thus not allowing for a θ-dependence of all three functions would imply, that none of these functions could be long-ranged. This would physically not be acceptable, since also the massless photon is described by a combination of these functions. Thus the 'Coulomb gauge' is inadequate in 0th order.

b) 'Physical gauge'

A better gauge for the 0th order approximation is the 'physical gauge'. Here the asymptotic condition (2.21) allows both functions $F_4(x,\theta)$ and $F_7(x,\theta)$ to be long-ranged, thus yielding the proper asymptotic behaviour for the electromagnetic field. Since in this gauge we have the condition

$$f_{5,0}(x) = f_{6,0}(x) \tag{3.3}$$

in addition to condition (3.2c), there remain only five independent functions $f_{i,0}(x)$ to be determined.

The energy of the sphaleron in the 0th order in the 'physical gauge' is shown as a function of the mixing angle in Fig.1a for $M_H = M_W$. In the 0th order the energy density is finite in this gauge. In the limit $\theta_w = \pi/2$, the variational principle yields the relation

$$f_{7,0}(x) = f_{4,0}(x)$$

c) Restricted calculation of ref. [17]

The results of Klinkhamer and Laterveer [17] are obtained, when in the 'physical gauge' the functions $f_{i,0}(x)$ are further restricted according to

$$f_{1,0}(x) = f_{2,0}(x) = f_{3,0}(x)\ . \tag{3.4}$$

This leaves only four functions to be determined. For comparison, we also show these results in Fig.1a for $M_H = M_W$.

3.2 Higher order Legendre polynomial expansion

We turn now to the general expansion in terms of Legendre polynomials. Following Rebbi and Rossi [16] we expand the functions $F_i(x,\theta)$ as follows

$$F_1(x,\theta) = f_{1,0}(x) + \sum_{l=2}^{2N} f_{1,l}(x) \frac{\cos^2\theta - 1}{l\cos\theta} \frac{dP_l(\cos\theta)}{d\cos\theta}\ , \tag{3.5a}$$

$$F_2(x,\theta) = f_{2,0}(x) + \sum_{l=2}^{2N} f_{2,l}(x) \frac{\cos\theta}{l} \frac{dP_l(\cos\theta)}{d\cos\theta}\ , \tag{3.5b}$$

$$F_3(x,\theta) = f_{1,0}(x) + \sum_{l=2}^{2N} f_{3,l}(x) \frac{\cos^2\theta - 1}{l\cos\theta} \frac{dP_l(\cos\theta)}{d\cos\theta}\ , \tag{3.5c}$$

$$F_4(x,\theta) = f_{4,0}(x) + \sum_{l=2}^{2N} f_{4,l}(x) \frac{\cos\theta}{l} \frac{dP_l(\cos\theta)}{d\cos\theta}\ , \tag{3.5d}$$

$$F_5(x,\theta) = f_{5,0}(x) + \sum_{l=2}^{2N} f_{5,l}(x) P_l(\cos\theta)\ , \tag{3.5e}$$

$$F_6(x,\theta) = f_{6,0}(x) + \sum_{l=2}^{2N} f_{6,l}(x) P_l(\cos\theta) \ , \qquad (3.5f)$$

$$F_7(x,\theta) = f_{7,0}(x) + \sum_{l=2}^{2N} f_{7,l}(x) P_l(\cos\theta) \ , \qquad (3.5g)$$

where l assumes only even values due to the parity reflection symmetry. The higher order terms in the expansion of $F_1(x,\theta)$ and $F_3(x,\theta)$ are proportional to $\sin^2\theta$, while for $F_2(x,\theta)$ and $F_4(x,\theta)$ they are proportional to $\cos^2\theta$. The constraint (3.2b) requires the condition (3.2c) for the 0th order functions in the expansion of $F_1(x,\theta)$ and $F_3(x,\theta)$, but the $\sin^2\theta$-dependence of the higher order terms in the expansion makes these contributions regular without the need for further constraining conditions.

We will put our main emphasis on the calculations in the 'Coulomb gauge', since these results will be directly compared with the corresponding results from the integration of the *partial* differential equations in section 4.

a) 'Coulomb gauge'

In contrast to the 0th order expansion, for the higher order expansions the 'Coulomb gauge' is an adequate choice of gauge, since the asymptotic relations (2.18) can now be satisfied with long-ranged fields. We have performed calculations in the 'Coulomb gauge' for expansions of 2nd, 4th and 6th order. This involves solving systems of $(6 + 7l/2)$ coupled *ordinary* differential equations. Obviously, the computational effort increases significantly with each order.

Let us first discuss the gauge invariant quantities, the energy, the energy density and the magnetic moment, as functions of the mixing angle θ_w. Fig.1 shows the energy of the electroweak sphaleron obtained in 0th order in the 'physical gauge', and in 2nd, 4th and 6th order in the 'Coulomb gauge' for $M_H = M_W$. The energy decreases as a function of the mixing angle, for small θ_w only slightly, for larger θ_w stronger. The higher order terms affect the energy only at larger values of the mixing angle. Each higher order lowers the energy only beyond increasingly larger values of θ_w. But in each order the energy reaches a finite lower limiting value for $\theta_w = \pi/2$.

Let us now consider the convergence of the expansion as illustrated in Fig.1. In Fig.1a we compare the energies from the 2nd order calculation in the 'Coulomb gauge' with the corresponding energies from the 0th order calculations in the 'physical gauge'. We observe, that up to quite large values of the mixing angle the 0th order approximation it remarkably good. At $\theta_w = 0.5$, the physical value of the mixing angle, the 0th order approximation yields an energy value only 0.001% higher than the 2nd order approximation, and the discrepancy increases only slowly. It is 0.01% at $\theta_w = 0.8$, 0.1% at $\theta_w = 1.1$ and reaches 3.7% in the limit $\theta_w = \pi/2$. The 4th order results are shown in Fig.1b. The energies of the 4th order expansion begin to deviate from those of the 2nd order expansion only at $\theta_w = 1.2$, where the difference is 0.001%. The 6th order results finally deviate from the 4th order results only beyond $\theta_w = 1.5$, reaching 0.001% at $\theta_w = 1.52$. They are illustrated in Fig.1c for large θ_w.

Let us now consider the energy density. In Figs.2a-d we illustrate the energy density as a function of the spatial coordinates x and θ, for the mixing angles $\theta_w = 0.5,\ 1.0,\ 1.5$

and 1.55, and for $M_H = M_W$. At the physical mixing angle $\theta_w = 0.5$ the energy density is hardly deformed and differs only little form the spherical energy density. Then with increasing mixing angle θ_w the sphaleron becomes more and more deformed. The energy density is larger along the z-axis (for angle $\theta = 0$) and smaller along the ρ-axis (for angle $\theta = \pi/2$). Equal density contours form ellipsoids, which become increasingly elongated in the z-direction for increasingly large values of the mixing angle.

The energy density at the origin, the central density, is shown as a function of the mixing angle in Fig.3 for $M_H = M_W$ for the 0th order calculation in the 'physical gauge' and for the 6th order calculation in the 'Coulomb gauge'. With increasing mixing angle the central density decreases first slightly. Then it reaches a minimum at $\theta_w \approx 1.2$. When the mixing angle approaches the value $\theta_w = \pi/2$, the central density (in the 'Coulomb gauge') diverges rapidly. The higher the order of the calculation the earlier the dramatic increase of the central density sets in.

Another interesting physical quantity characterizing the electroweak sphaleron is its magnetic dipole moment μ. The electromagnetic field of the electroweak sphaleron has the asymptotic behaviour

$$\vec{A}_{EM}(\vec{r}) \to \frac{\vec{\mu} \times \vec{r}}{4\pi r^3} , \tag{3.6a}$$

where $\vec{\mu} = (0, 0, \mu)$ represents the magnetic dipole moment. It can be extracted from the long-range behaviour of the functions $F_3(x,\theta)$, $F_4(x,\theta)$ and $F_7(x,\theta)$. To extract this magnetic dipole moment we perform an (asymptotic) gauge transformation, which changes the asymptotically twisted Higgs field in the 'Coulomb gauge' to the 'physical gauge'. Applying this transformation to the SU(2) gauge field yields the 'physical' asymptotic isospin-3 component of the gauge field, needed to construct the asymptotic behaviour of the electromagnetic field and of the massive Z^0-field. The magnetic dipole moment is then obtained as

$$\mu = \frac{e}{\alpha_w M_W} \Xi \quad , \quad \Xi = x F_7(x) \frac{g^2}{e^2} \quad (x \to \infty) . \tag{3.6b}$$

The magnetic dipole moment as a function of the mixing angle is shown in Fig.4 for $M_H = M_W$ for the 0th order calculation in the 'physical gauge' and for the 2nd, 4th and 6th order calculations in the 'Coulomb gauge'. The convergence properties of the expansion as a function of the mixing angle θ_w are for the magnetic dipole moment similar to those for the energy discussed above. At the physical value of the mixing angle we find a magnetic dipole moment, which is only slightly different from the value obtained by Klinkhamer and Manton [6] applying perturbation theory. Thus we confirm their remarkable result, that the electroweak sphaleron has a very big magnetic dipole moment.

We finally turn to the functions $F_i(x,\theta)$ themselves, which are gauge-dependent except for the U(1) field function $F_7(x,\theta)$ and the length function of the Higgs field $L(x,\theta)$

$$L(x,\theta) = \sqrt{F_5(x,\theta)^2 \sin^2\theta + F_6(x,\theta)^2 \cos^2\theta} .$$

Figs.5-8 show the functions $F_1(x,\theta)$ and $F_2(x,\theta)$, $F_3(x,\theta)$ and $F_4(x,\theta)$, $F_5(x,\theta)$ and $F_6(x,\theta)$, $F_7(x,\theta)$ and $L(x,\theta)$, obtained with calculations of the 6th order, for the mixing angles $\theta_w = 0.5,\ 1.0,\ 1.5$ and 1.55 and for $M_H = M_W$. The figures clearly demonstrate the effect which an increase of the mixing angle has on the functions.

At $\theta_w = 0.5$ there is hardly any angular θ-dependence noticable in the functions $F_i(x,\theta)$, except for the trivial asymptotic θ-dependence of $F_3(x,\theta)$ and $F_4(x,\theta)$, implied by the asymptotic relations (2.18). At $\theta_w = 1.0$ a noticable non-trivial θ-dependence of the functions $F_i(x,\theta)$ in the inner region of the sphaleron has developped and keeps increasing with increasing mixing angle.

We observe, that at the origin with increasing mixing angle the functions $F_1(x,\theta)$ and $F_2(x,\theta)$ tend more and more apart from each other, and likewise the functions $F_5(x,\theta)$ and $F_6(x,\theta)$. For the latter we further observe, that for $\theta_w \to \pi/2$ the slope of $F_5(x,\theta)$ at the origin tends to infinity, while the slope of $F_6(x,\theta)$ tends to zero,

$$\frac{dF_5(x,\theta)}{dx} \underset{x\to 0}{\longrightarrow} \infty\ , \tag{3.7a}$$

$$\frac{dF_6(x,\theta)}{dx} \underset{x\to 0}{\longrightarrow} 0\ . \tag{3.7b}$$

It is this behaviour (3.7a) of the Higgs field, which leads to the divergence of the energy density at the origin in the limit $\theta_w \to \pi/2$.

For very large values of the mixing angle the most dramatic changes appear in the functions $F_5(x,\theta)$, $F_6(x,\theta)$ and $F_7(x,\theta)$. In particular, for small angles θ the functions $F_5(x,\theta)$ and $F_7(x,\theta)$ develop pronounced peaks. This is demonstrated in Figs.9-10, where for comparison we present the 4th and the 6th order results for the mixing angles $\theta_w = 1.55,\ 1.56$ and 1.57.

Comparing all the results obtained in the various orders we conclude, that the 0th order approximation in the 'physical gauge' is excellent up to the physical value of the mixing angle $\theta_w = 0.5$. In the 'Coulomb gauge' the 2nd order approximation is as good and fully sufficient up to $\theta_w = 1.2$ and the 4th order approximation up to $\theta_w = 1.52$. Up to which value of the mixing angle the 6th order calculation does well, we will see in section 4, where we compare with the results obtained by directly integrating the *partial* differential equations. For very large values of the mixing angle the expansion obviously has not yet converged.

b) Gauge fixing by elimination of contraints

To discuss the second gauge used for the higher order expansion, let us return to eqs.(3.5). Inserting this expansion of the functions $F_i(x,\theta)$ into the energy functional (2.7), where no gauge fixing condition has as yet been chosen, we find, that for the lth order expansion there are only (6+6l/2) independent propagating functions, accompanied by (l/2) constraints which arise for combinations of the functions $f_{1,l}(x)$ and $f_{2,l}(x)$. Rewriting these functions for $l > 0$ as the combinations

$$f_{1,l}(x) = \tilde{f}_{1,l}(x) + \tilde{f}_{2,l}(x)\ , \tag{3.8a}$$

$$f_{2,l}(x) = \tilde{f}_{1,l}(x) - \tilde{f}_{2,l}(x) \ , \tag{3.8b}$$

we see, that the energy functional does not contain the derivatives of the functions $\tilde{f}_{1,l}(x)$. Therefore they lead only to constraint equations. Having isolated the constraints, we fix the gauge by demanding

$$\tilde{f}_{1,l}(x) = 0 \ . \tag{3.9}$$

This choice simplifies the set of *ordinary* differential equations considerably.

For gauge independent quantities the results obtained in this gauge are in excellent agreement with those obtained in the 'Coulomb gauge'. Also the gauge-dependent functions $F_i(x,\theta)$ show in this gauge many features similar to the 'Coulomb gauge'. For instance, the functions $F_1(x,\theta)$ and $F_2(x,\theta)$ and also $F_5(x,\theta)$ and $F_6(x,\theta)$ split increasingly strongly at the origin with increasing mixing angle θ_w. But the angular θ-dependence of the functions $F_1(x,\theta)$ and $F_2(x,\theta)$, and $F_5(x,\theta)$ and $F_6(x,\theta)$ themselves remains smaller than in the 'Coulomb gauge'. In particular, $F_5(x,\theta)$ does not develop the peak along the z-axis for very large values of the mixing angle. As an example we present the functions $F_i(x,\theta)$ for $\theta_w = 1.5$ and for $M_H = M_W$ in Fig.11.

c) 'Hedgehog gauge' and 'physical gauge'

In contrast to the 0th order calculation, where the 'physical gauge' does quite well, it becomes inappropriate for the higher orders. As we have seen for the gauges discussed above, a non-vanishing mixing angle leads to the splitting of the Higgs field functions $F_5(x,\theta)$ and $F_6(x,\theta)$ at the origin. In the 'hedgehog gauge' and likewise in the 'physical gauge', however, we require, that the Higgs field functions $F_5(x,\theta)$ and $F_6(x,\theta)$ are equal to one another, eq.(2.19). This condition proves to be too strong. In fact, requiring condition (2.19) for the Higgs field functions leads to an unacceptable behaviour for the functions $f_{i,l}(x)$ at the origin, describing the SU(2) gauge field. Instead of the expected regular behaviour at the origin,

$$f_{i,l}(x) \to c_i x^l \ , \tag{3.10}$$

we observe, that several of the functions $f_{i,l}(x)$ rise only with a lower power of x at the origin. This yields functions $F_i(x,\theta)$, not well-defined at the origin. As a consequence of this bad behaviour of the SU(2) gauge field functions at the origin, the energy density is not well-defined at the origin either but diverges, for any $\theta_w \neq 0$. This will be demonstrated in the next section.

4. Results: Partial differential equations

We now present the results for the electroweak sphaleron obtained by integrating directly the set of coupled non-linear *partial* differential equations numerically. The calculations cover the range of the mixing angle $0 \leq \theta_w < \pi/2$. We consider several choices of gauge, but put the main emphasis on the 'Coulomb gauge'.

The numerical calculations are based on the Newton-Raphson method [18]. The equations are discretized on a non-equidistant grid in x and an equidistant grid in θ. For

small mixing angles θ_w grids of sizes 50×20 and 100×20 are used, covering integration regions $0 < x < 40$ and $0 < x < 120$, with $0 < \theta < \pi/2$. For large values of θ_w the number of grid points in θ is doubled to obtain the functions $F_i(x, \theta)$ with high accuracy, i.e. a relative numerical error estimated to be smaller than 10^{-3}. However, for mixing angles very close to the limiting value $\theta_w = \pi/2$, even the larger grid size does not lead to a high numerical accuracy, and thus reliable results. In fact, for mixing angles $\theta_w > 1.567$ the numerical results have a relative error on the order of 10^{-2} or even bigger for some of the functions $F_i(x, \theta)$. In particular, the error for the functions $F_5(x, \theta)$ and $F_7(x, \theta)$ along the z-axis increases considerably. Our calculations are therefore much less reliable for θ_w very close to $\pi/2$. Consequently we cannot determine the limiting sphaleron configuration and its properties for $\theta_w = \pi/2$.

a) 'Coulomb gauge'

The numerical results for the sphaleron at finite mixing angle obtained by solving the *partial* differential equations in the 'Coulomb gauge' agree (within our numerical accuracy) with the corresponding results from the highest order Legendre polynomial expansion up to very large values of the mixing angle. This is demonstrated for the energies for $M_H = M_W$ in Fig.12, where deviations between the 6th order calculation and the numerical integration of the *partial* differential equations become visible only beyond $\theta_w = 1.54$. Since for $\theta_w > 1.567$ the numerical accuracy of the calculations becomes increasingly worse, these results are indicated by a dotted curve only. Due to the lack of accuracy we unfortunately cannot definitely decide, whether the energy of the sphaleron remains finite in the limit $\theta_w \to \pi/2$, although concluding from the polynomial expansion this appears to be the case. The limiting value of the energy for $\theta_w = \pi/2$ remains thus unknown.

Also the energy densities agree with those from the polynomial expansion up to $\theta_w = 1.54$. Beyond this value of the mixing angle, the energy density obtained by solving the *partial* differential equations increases stronger at the origin and thus diverges faster. The value of the energy density at the origin is shown in Fig.13 for θ_w close to $\pi/2$ for $M_H = M_W$. Again, the less accurate results are indicated only by a dotted curve. For comparison the energy densities obtained with the 0th order ('physical gauge') and with the 6th order ('Coulomb gauge') calculations are also shown. (Note the logarithmic scale.)

For the functions $F_i(x, \theta)$ deviations between the 6th order calculation ('Coulomb gauge') and the numerical integration of the *partial* differential equations begin to appear beyond $\theta_w = 1.54$ as well. Again, the deviations are most apparent for the functions $F_5(x, \theta)$ and $F_7(x, \theta)$ along the z-axis. The peaks in these functions develop earlier and more rapidly at large values of the mixing angle, as compared to the 6th order polynomial calculations. This is demonstrated with the help of Fig.14, where these functions obtained by solving the *partial* differential equations are shown. The functions of Fig.14 should be compared with those of Figs.9-10.

Thus we conclude, that for $\theta_w \geq 1.54$ higher than 6th order terms in the polynomial expansion are necessary for an accurate description of the sphaleron. The construction of the sphaleron in the limit $\theta_w = \pi/2$ remains a numerically challenging task.

b) 'Hedgehog gauge' and 'physical gauge'

As discussed for the polynomial expansion in section 3, for finite values of the mixing angle the 'hedgehog gauge' and the 'physical gauge' lead to gauge field functions $F_i(x,\theta)$, which are not well-defined at the origin,

$$\left.\frac{\partial F_i(x,\theta)}{\partial x}\right|_{x=0} = f_i(\theta) \neq const \ , \tag{4.1}$$

i.e. the derivatives are not single-valued at the origin but depend on the angle θ instead. A finite energy density at the origin, however, requires, that the gauge field functions as well as their derivatives vanish at the origin. Therefore these gauges lead to energy densities, which diverge at the origin, for any finite value of the mixing angle θ_w. As an example, we illustrate the energy density for the physical mixing angle $\theta_w = 0.5$ in Fig.15. Even at this small mixing angle, where the 0th order expansion in the 'physical gauge' does very well for the energy, the very slight θ-dependence of the functions $F_i(x,\theta)$ close to the origin leads to a dramatic effect for the energy density in the vicinity of the origin. (Compare with Fig.2a.) The dependence of the energy density on the angle θ in the vicinity of the origin becomes even much stronger for larger values of the mixing angle θ_w. Thus these gauges are inadequate choices for the electroweak sphaleron.

5. Conclusions

We have constructed the classical sphaleron solution of the Weinberg-Salam theory for finite values of the mixing angle, $0 \leq \theta_w \leq \pi/2$. For the numerical calculations we have applied two alternative methods.

1. We have converted the system of coupled non-linear *partial* differential equations by means of a Legendre polynomial expansion into a system of *ordinary* differential equations and solved this system with 0th order up to 6th order polynomials included.
2. We have solved the system of coupled non-linear *partial* differential equations directly.

Comparing the results obtained by the two methods we have found, that the 0th order expansion in the 'physical gauge' is very good for small mixing angles, even up to the physical value of the mixing angle, $\theta_w = 0.5$. Choosing the 'Coulomb gauge' beyond, the 2nd order expansion is sufficient up to $\theta_w \leq 1.2$, the 4th order up to $\theta_w \leq 1.52$ and the 6th order for $\theta_w \leq 1.54$. Then 8th and higher order terms must be included.

For the polynomial expansion we have been able to achieve a high numerical accuracy over the whole range of values of the mixing angle $0 \leq \theta_w \leq \pi/2$, but we had to limit ourselves to expansions of order $l \leq 6$. For the direct integration of the *partial* differential equations we have been able to achieve a high numerical accuracy only for values of the mixing angle up to $\theta_w \leq 1.567$, and not all the way to the limiting value $\theta_w = \pi/2$. Thus the interesting questions, what the limiting sphaleron solution looks like and whether it has a finite energy, remain open.

While at vanishing mixing angle $\theta_w = 0$ the energy density of the sphaleron is spherical, it becomes spheroidal for finite values of the mixing angle. Equal density

contours, represented by ellipsoids, become elongated in the z-direction, and the ratio of major and minor half-axes increases with increasing mixing angle.

As the energy density deforms more and more strongly, the total energy of the sphaleron decreases with increasing mixing angle. The larger the mixing angle the faster this decrease becomes. At the physical value of the mixing angle, $\theta_w = 0.5$, the energy has decreased only by about 1% compared to the spherical case. At $\theta_w = 1.0$ and $\theta_w = 1.5$ it has decreased by about 4% and 14%, respectively, and even at $\theta_w = 1.567$, our largest reliable value, the energy has only decreased by about 17%. This relative weak dependence of the energy on the mixing angle is seen throughout the considered range of values of the Higgs mass, $1/2M_W \leq M_H \leq 10M_W$.

Solutions of non-linear equations, when considered as functions of an external parameter, often exist only up to a critical value of this parameter, where a bifurcation is encountered. Due to this phenomenon extrapolations for such solutions must be regarded with caution. In the case of the sphaleron with as external parameter the mixing angle we have not encountered a critical point, beyond which the solution ceases to exist. In contrary, the sphaleron has continuously deformed throughout the full range of this parameter, $0 \leq \theta_w < \pi/2$. In fact, the estimate of Klinkhamer and Manton [6] of the effect, which the finite physical value of the mixing angle would have on the sphaleron, has turned out to be remarkably good.

All previous calculations on baryon number violation in the early universe [7-10] have applied the spherical approximation of the electroweak sphaleron, neglecting the effects of the finite physical value of the mixing angle. Our analysis has shown, that this approximation is very good, as far as the classical solution is concerned. We expect, that also the analysis of the normal modes of oscillation around the true electroweak sphaleron solution will differ little from the analysis around the spherical, approximate solution [9,15,19-20]. We therefore expect, that the previous calculations and conclusions on baryon number violation in the early universe [7-10] will remain valid, at least with respect to the spherical approximation of the electroweak sphaleron employed there.

Since non-linear systems often hold surprises, however, a definite conclusion on this very important aspect clearly requires performing the mode analysis around the axially symmetric sphaleron. After all, new instabilities of the sphaleron and associated new classical solutions might arise as the mixing angle increases from the spherical limit to the physical value and beyond.

Acknowledgement

One of us (J. K.) gratefully acknowledges discussions with G. 't Hooft, L. Wilets and L. Yaffe and support from the Netherlands Organization for Scientific Research (NWO) and the Institute for Nuclear Theory (INT) Seattle.

6. References

[1] G. 't Hooft, Phys. Rev. Lett. 37 (1976) 8.

[2] S. L. Adler, Phys. Rev. 177 (1969) 2926;
J. S. Bell and R. Jackiw, Nuovo Cim. 60 (1969) 47;
W. A. Bardeen, Phys. Rev. 189 (1969) 1848.

[3] *Baryon Number Violation at the SSC?*, Santa Fe Workshop, eds. M. Mattis and E. Mottola (World Scientific, Singapore, 1990).

[4] A. Ringwald, Nucl. Phys. B330 (1990) 1.

[5] N. S. Manton, Phys. Rev. D28 (1983) 2019.

[6] F. R. Klinkhamer and N. S. Manton, Phys. Rev. D30 (1984) 2212.

[7] V. Kuzmin, V. Rubakov and M. Shaposhnikov, Phys. Lett. 155B (1985) 36.

[8] P. Arnold and L. McLerran, Phys. Rev. D36 (1987) 581; D37 (1988) 1020;
L. Carson and L. McLerran, Phys. Rev. D41 (1990) 647;
L. Carson, Xu Li, L. McLerran and R.-T. Wang, Phys. Rev. D42 (1990) 2127.

[9] A. Ringwald, Phys. Lett. B201 (1988) 510;
J. Kripfganz and A. Ringwald, Z. Phys. C44 (1989) 213.

[10] *The Early Universe*, E. W. Kolb and M. S. Turner (Addison-Wesley Publishing Company, Redwood City, 1990).

[11] R. Dashen, B. Hasslacher and A. Neveu, Phys. Rev. D10 (1974) 4138.

[12] B. Kleihaus, J. Kunz and Y. Brihaye, Phys. Lett. 273B (1991) 100.

[13] N. S. Manton, Nucl. Phys. B135 (1978) 319.

[14] J. Kunz and Y. Brihaye, Phys. Lett. 216B (1989) 353.

[15] L. G. Yaffe, Phys. Rev. D40 (1989) 3463.

[16] C. Rebbi and P. Rossi, Phys. Rev. D22 (1980) 2010.

[17] F. R. Klinkhamer and R. Laterveer, NIKHEF-H/90-12.

[18] W. Schönauer and E. Schnepf, Parallel Computing 6 (1988) 185.

[19] T. Akiba, H. Kikuchi and T. Yanagida, Phys. Rev. D40 (1989) 179.

[20] Y. Brihaye and J. Kunz, Phys. Lett. 249B (1990) 90; Y. Brihaye and J. Kunz, preprint (1991).

7. Figure Captions

Fig. 1a:

The energy of the sphaleron (in units of TeV) is shown as a function of the mixing angle θ_w for $M_H = M_W$. The solid curve represents the 0th order calculation ('physical gauge'), the dashed curve represents the 2nd order calculation ('Coulomb gauge') and the dotted curve represents the approximation of ref. [17].

Fig. 1b:

Idem Fig. 1a; solid curve: 0th order calculation ('physical gauge'), dashed curve: 2nd order calculation ('Coulomb gauge'), dot-dashed curve: 4th order calculation ('Coulomb gauge').

Fig. 1c:

Idem Fig. 1a; dashed curve: 2nd order calculation ('Coulomb gauge'), dot-dashed curve: 4th order calculation ('Coulomb gauge'), solid curve: 6th order calculation ('physical gauge').

Fig. 2a:

The energy density of the sphaleron (in units of M_W/α_w) obtained in the 6th order calculation ('Coulomb gauge') is shown as a function of the dimensionless coordinate x at $\theta_w = 0.5$ for $M_H = M_W$. The solid and the dashed curves represent the angles $\theta = 0$ and $\theta = \pi/2$, respectively. For comparison, the dotted curve represents the energy density of the spherical sphaleron at $\theta_w = 0$.

Fig. 2b:

Idem Fig. 2a for $\theta_w = 1.0$; solid curve: angle $\theta = 0$, dotted curve: angle $\theta = \pi/4$, dashed curve: angle $\theta = \pi/2$.

Fig. 2c:

Idem Fig. 2a for $\theta_w = 1.5$; solid curve: angle $\theta = 0$, dotted curve: angle $\theta = \pi/4$, dashed curve: angle $\theta = \pi/2$.

Fig. 2d:

Idem Fig. 2a for $\theta_w = 1.55$; solid curve: angle $\theta = 0$, dotted curve: angle $\theta = \pi/4$,

Fig. 3:

The energy density of the sphaleron at the origin (in units of M_W/α_w) is shown as a function of the mixing angle θ_w for $M_H = M_W$. The dashed curve represents the 0th order calculation ('physical gauge'), and the solid curve represents the 6th order calculation ('Coulomb gauge').

Fig. 4:

The magnetic dipole moment of the sphaleron (in units of $e/\alpha_w M_W$) is shown as a function of the mixing angle θ_w for $M_H = M_W$. The dashed curve represents the 0th order calculation ('physical gauge'), the dot-dashed curve represents the 2nd order calculation ('Coulomb gauge'), the dotted curve represents the 4th order calculation ('Coulomb gauge'), and the solid curve represents the 6th order calculation ('Coulomb gauge').

Fig. 5a:

The SU(2) gauge field functions $F_1(x,\theta)$ and $F_2(x,\theta)$ obtained in the 6th order calculation ('Coulomb gauge') are shown as a function of the dimensionless coordinate x at $\theta_w = 0.5$ for $M_H = M_W$. The solid and the dashed curves represent the angles $\theta = 0$ and $\theta = \pi/2$, respectively. The curves for $F_1(x,\theta)$ are slightly below those for $F_2(x,\theta)$. (See the larger mixing angles.)

Fig. 5b:

Idem Fig. 5a for $\theta_w = 1.0$; solid curves: angle $\theta = 0$, dashed curves: angle $\theta = \pi/2$.

Fig. 5c:

Idem Fig. 5a for $\theta_w = 1.5$; solid curves: angle $\theta = 0$, dotted curves: angle $\theta = \pi/4$, dashed curves: angle $\theta = \pi/2$.

Fig. 5d:

Idem Fig. 5a for $\theta_w = 1.55$; solid curves: angle $\theta = 0$, dotted curves: angle $\theta = \pi/4$, dashed curves: angle $\theta = \pi/2$.

Fig. 6a:

The SU(2) gauge field functions $F_3(x,\theta)$ and $F_4(x,\theta)$ obtained in the 6th order calculation ('Coulomb gauge') are shown as a function of the dimensionless coordinate x at $\theta_w = 0.5$ for $M_H = M_W$. The solid, the dotted and the dashed curves represent the angles $\theta = 0$, $\theta = \pi/4$ and $\theta = \pi/2$, respectively. (See the larger mixing angles.)

Fig. 6b:

Idem Fig. 6a for $\theta_w = 1.0$; solid curves: angle $\theta = 0$, dotted curves: angle $\theta = \pi/4$, dashed curves: angle $\theta = \pi/2$.

Fig. 6c:

Idem Fig. 6a for $\theta_w = 1.5$; solid curves: angle $\theta = 0$, dotted curves: angle $\theta = \pi/4$, dashed curves: angle $\theta = \pi/2$.

Fig. 6d:

Idem Fig. 6a for $\theta_w = 1.55$; solid curves: angle $\theta = 0$, dotted curves: angle $\theta = \pi/4$, dashed curves: angle $\theta = \pi/2$.

Fig. 7a:

The Higgs field functions $F_5(x,\theta)$ and $F_6(x,\theta)$ obtained in the 6th order calculation ('Coulomb gauge') are shown as a function of the dimensionless coordinate x at $\theta_w = 0.5$ for $M_H = M_W$. The solid and the dashed curves represent the angles $\theta = 0$ and $\theta = \pi/2$, respectively. The curves for $F_5(x,\theta)$ are slightly above those for $F_6(x,\theta)$. (See the larger mixing angles.)

Fig. 7b:

Idem Fig. 7a for $\theta_w = 1.0$; solid curves: angle $\theta = 0$, dashed curves: angle $\theta = \pi/2$.

Fig. 7c:

Idem Fig. 7a for $\theta_w = 1.5$; solid curves: angle $\theta = 0$, dotted curves: angle $\theta = \pi/4$, dashed curves: angle $\theta = \pi/2$.

Fig. 7d:

Idem Fig. 7a for $\theta_w = 1.55$; solid curves: angle $\theta = 0$, dotted curves: angle $\theta = \pi/4$, dashed curves: angle $\theta = \pi/2$.

Fig. 8a:

The U(1) gauge field function $F_7(x,\theta)$ and the length function of the Higgs field $L(x,\theta)$ obtained in the 6th order calculation ('Coulomb gauge') are shown as a function of the dimensionless coordinate x at $\theta_w = 0.5$ for $M_H = M_W$. The solid and the dashed curves represent the angles $\theta = 0$ and $\theta = \pi/2$, respectively.

Fig. 8b:

Idem Fig. 8a for $\theta_w = 1.0$; solid curves: angle $\theta = 0$, dashed curves: angle $\theta = \pi/2$.

Fig. 8c:

Idem Fig. 8a for $\theta_w = 1.5$; solid curves: angle $\theta = 0$, dotted curves: angle $\theta = \pi/4$, dashed curves: angle $\theta = \pi/2$.

Fig. 8d:

Idem Fig. 8a for $\theta_w = 1.55$; solid curves: angle $\theta = 0$, dotted curves: angle $\theta = \pi/4$, dashed curves: angle $\theta = \pi/2$.

Fig. 9a:

The Higgs field function $F_5(x,\theta)$ obtained in the 4th order calculation ('Coulomb gauge') is shown as a function of the dimensionless coordinate x at angle $\theta = 0$ for $M_H = M_W$. The dashed, dotted and solid curves represent the mixing angles $\theta_w = 1.55$, $\theta_w = 1.56$ and $\theta_w = 1.57$, respectively.

Fig. 9b:

Idem Fig. 9a for the 6th order calculation ('Coulomb gauge'); dashed curve: mixing angle $\theta_w = 1.55$, dotted curve: mixing angle $\theta_w = 1.56$, solid curve: mixing angle $\theta_w = 1.57$.

Fig. 10a:

The U(1) gauge field function $F_7(x,\theta)$ obtained in the 4th order calculation ('Coulomb gauge') is shown as a function of the dimensionless coordinate x at angle $\theta = 0$ for $M_H = M_W$. The dashed, dotted and solid curves represent the mixing angles $\theta_w = 1.55$, $\theta_w = 1.56$ and $\theta_w = 1.57$, respectively.

Fig. 10b:

Idem Fig. 10a for the 6th order calculation ('Coulomb gauge'); dashed curve: mixing angle $\theta_w = 1.55$, dotted curve: mixing angle $\theta_w = 1.56$, solid curve: mixing angle $\theta_w = 1.57$.

Fig. 11a:

The SU(2) gauge field functions $F_1(x,\theta)$ and $F_2(x,\theta)$ obtained in the 4th order calculation with gauge fixing by eliminating the constraint functions (3.9) are shown as a function of the dimensionless coordinate x at $\theta_w = 1.5$ for $M_H = M_W$. The solid and the dashed curves represent the angles $\theta = 0$ and $\theta = \pi/2$, respectively.

Fig. 11b:

Idem Fig. 11a for the SU(2) gauge field functions $F_3(x,\theta)$ and $F_4(x,\theta)$; solid curves: angle $\theta = 0$, dotted curves: angle $\theta = \pi/4$, dashed curves: angle $\theta = \pi/2$.

Fig. 11c:

Idem Fig. 11a for the Higgs field functions $F_5(x,\theta)$ and $F_6(x,\theta)$; solid curves: angle $\theta = 0$, dotted curves: angle $\theta = \pi/4$, dashed curves: angle $\theta = \pi/2$.

Fig. 11d:

Idem Fig. 11a for the U(1) gauge field function $F_7(x,\theta)$ and the length function of the Higgs field $L(x,\theta)$; solid curves: angle $\theta = 0$, dotted curves: angle $\theta = \pi/4$, dashed curves: angle $\theta = \pi/2$.

Fig. 12:

The energy of the sphaleron (in units of TeV) is shown as a function of the mixing angle θ_w for $M_H = M_W$. The solid curve represents the results with high accuracy and the dotted curve those with less accuracy, obtained by integrating the partial differential equations ('Coulomb gauge'). The long-dashed curve represents the 6th order calculation ('Coulomb gauge').

Fig. 13:

The energy density of the sphaleron at the origin (in units of M_W/α_w) is shown as a function of the mixing angle θ_w for $M_H = M_W$. The solid curve represents the results with high accuracy and the dotted curve those with less accuracy, obtained by integrating the partial differential equations ('Coulomb gauge'). The long-dashed curve represents the 6th order calculation ('Coulomb gauge'), and the short-dashed curve the 0th order calculation ('physical gauge').

Fig. 14a:

The Higgs field function $F_5(x,\theta)$ obtained by integrating the partial differential equations ('Coulomb gauge') is shown as a function of the dimensionless coordinate x at angle $\theta = 0$ for $M_H = M_W$. The dashed, dotted and solid curves represent the mixing angles $\theta_w = 1.55$, $\theta_w = 1.56$ and $\theta_w = 1.565$, respectively.

Fig. 14b:

Idem Fig. 14a for the U(1) gauge field function $F_7(x,\theta)$; dashed curve: mixing angle $\theta_w = 1.55$, dotted curve: mixing angle $\theta_w = 1.56$, solid curve: mixing angle $\theta_w = 1.565$.

Fig. 15:

The energy density of the sphaleron (in units of M_W/α_w) obtained by integrating the partial differential equations in the 'Hedgehog gauge' is shown as a function of the dimensionless coordinate x at $\theta_w = 0.5$ for $M_H = M_W$. The solid, dotted and dashed curves represent the angles $\theta = 0$, $\theta = \pi/4$ and $\theta = \pi/2$, respectively.

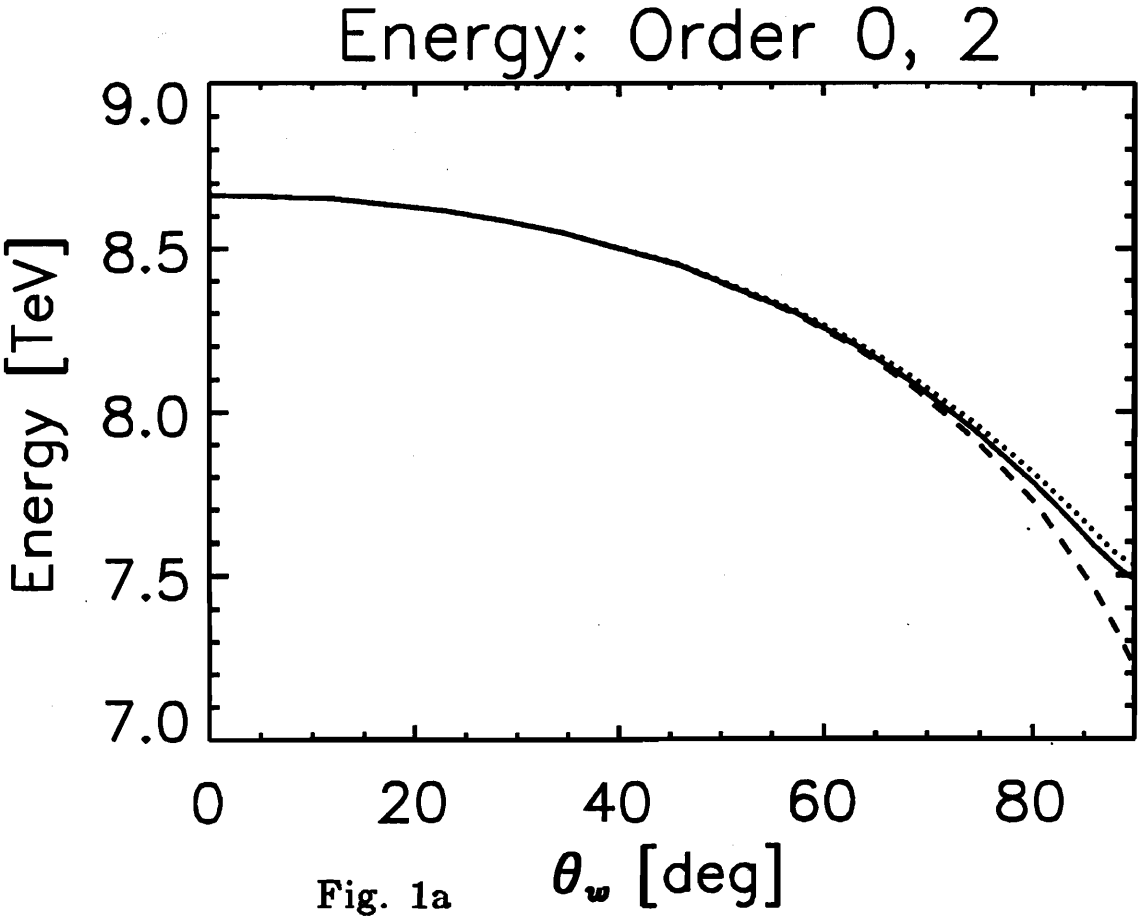
Energy: Order 0, 2
9.0
8.5
8.0
7.5
7.0
Energy [TeV]
0
20
40
60
80
θ_w [deg]

Fig. 1a

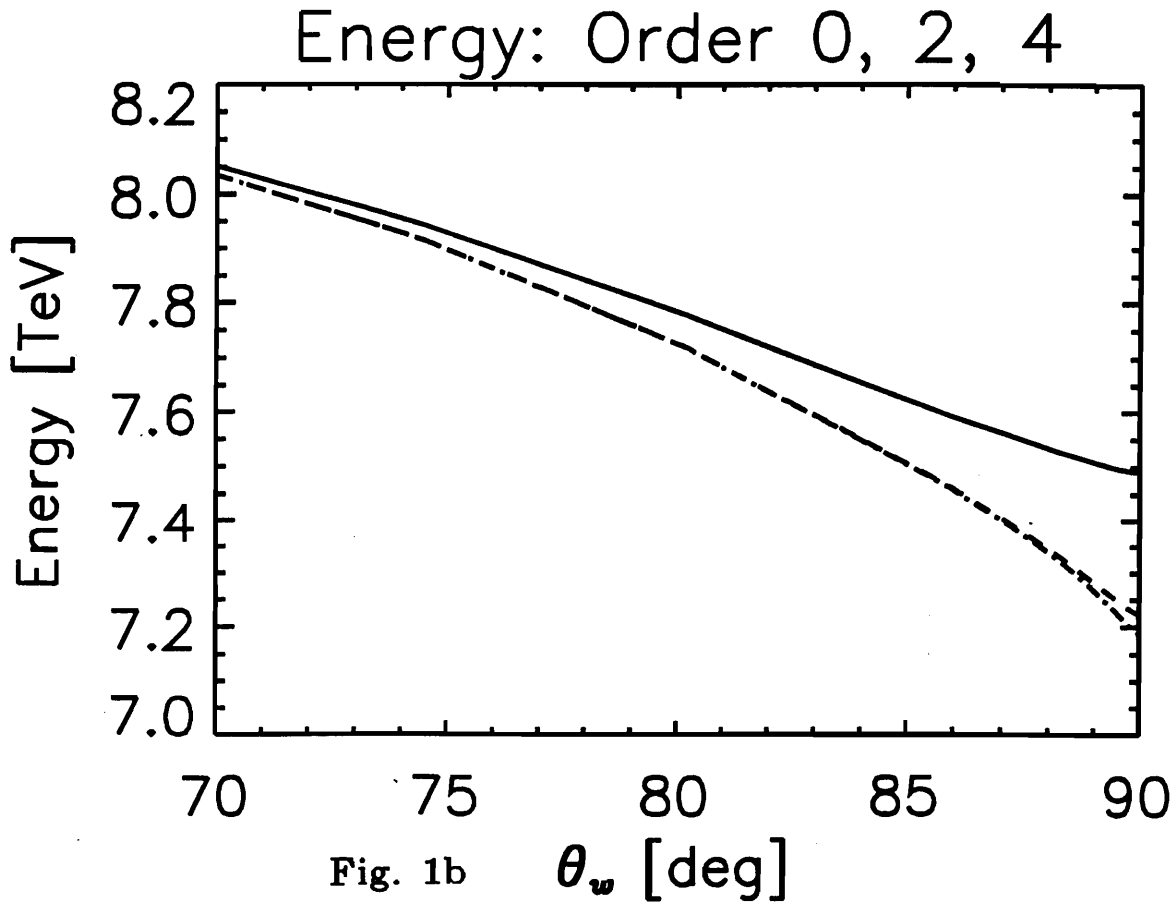
Energy: Order 0, 2, 4
8.2
8.0
7.8
7.6
7.4
7.2
7.0
Energy [TeV]
70
75
80
85
90
θ_w [deg]

Fig. 1b

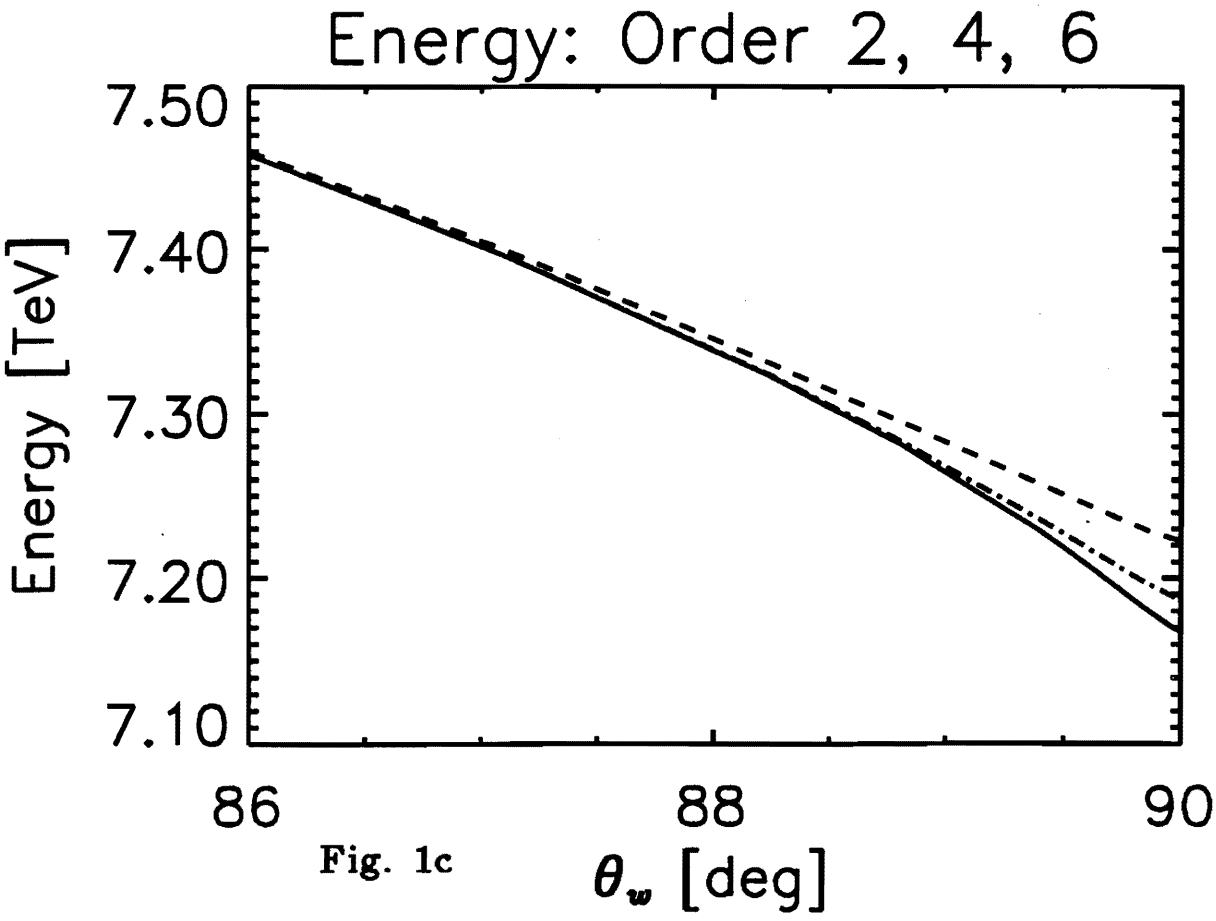
Energy: Order 2, 4, 6
7.50
7.40
7.30
7.20
7.10
Energy [TeV]
86
88
90
θ_w [deg]

Fig. 1c

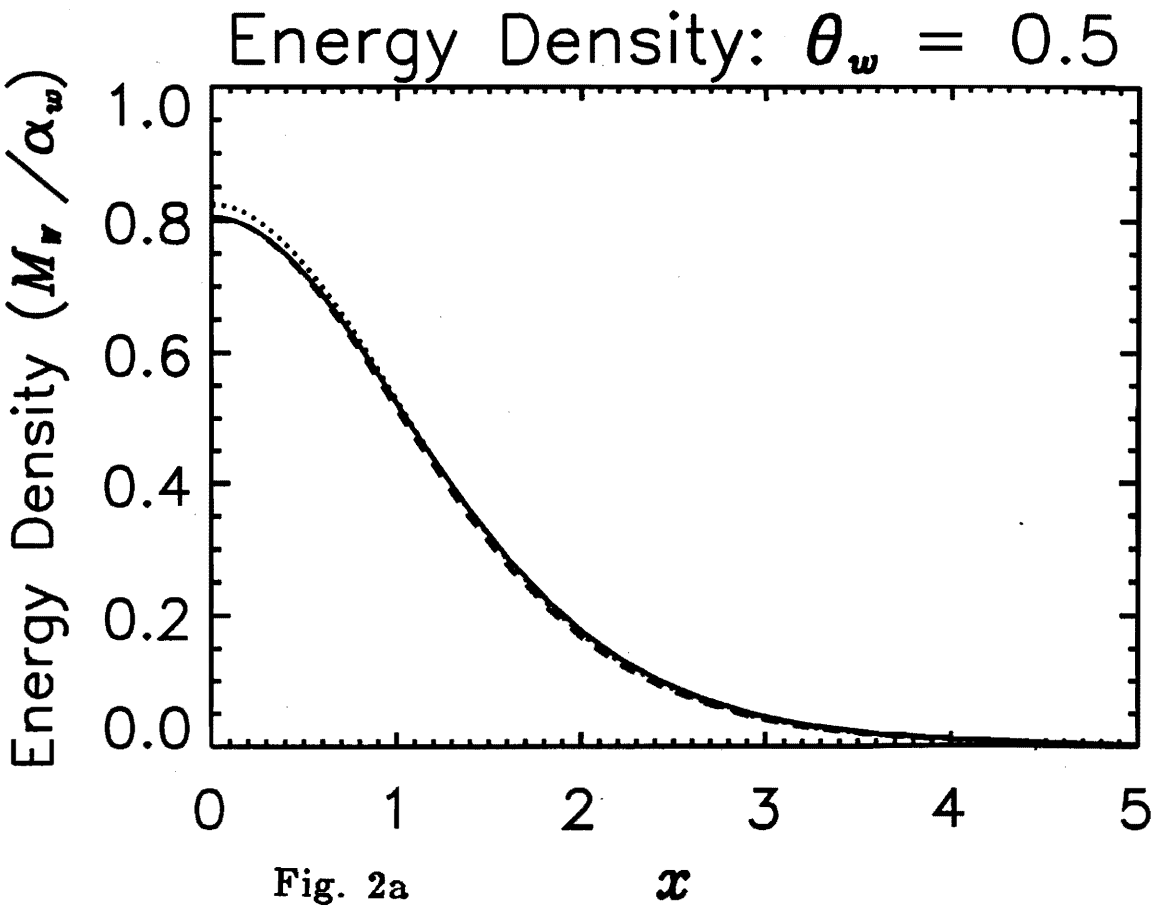
Energy Density: $\theta_w = 0.5$
Energy Density (M_r/α_w)
1.0
0.8
0.6
0.4
0.2
0.0
0
1
2
3
4
5
x

Fig. 2a

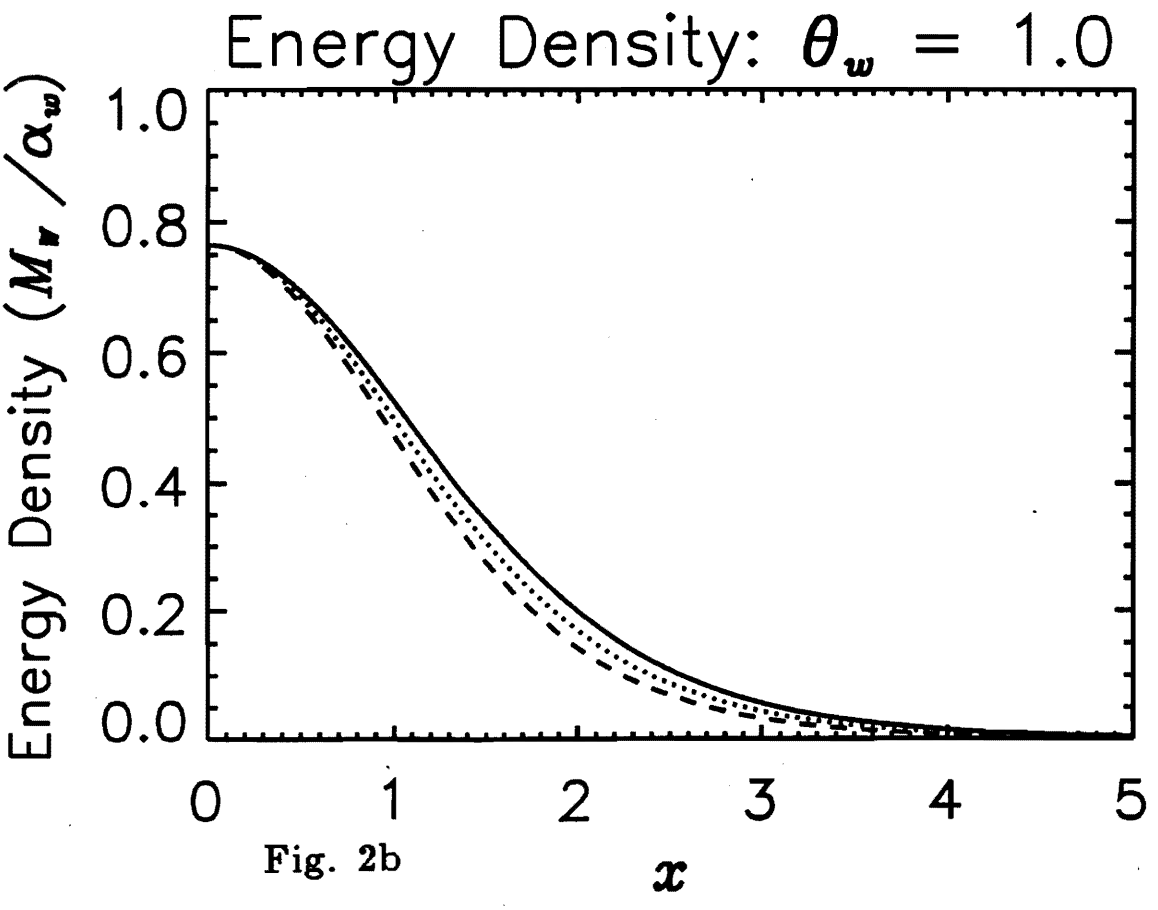
Energy Density: $\theta_w = 1.0$
Energy Density (M_r/α_w)
1.0
0.8
0.6
0.4
0.2
0.0
0
1
2
3
4
5
x

Fig. 2b

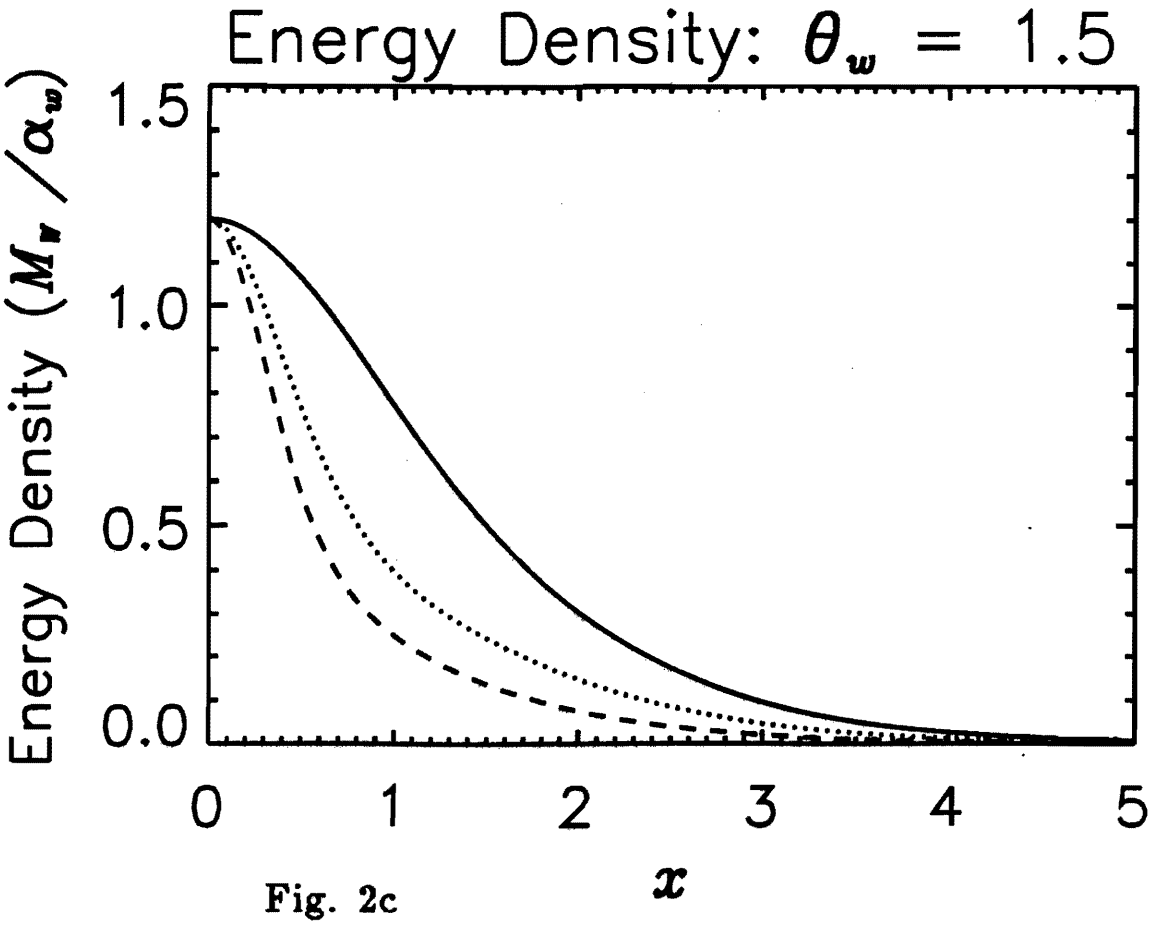
Energy Density: θ_w = 1.5
Energy Density (M_r /α_w)
1.5
1.0
0.5
0.0
0
1
2
3
4
5
x

Fig. 2c

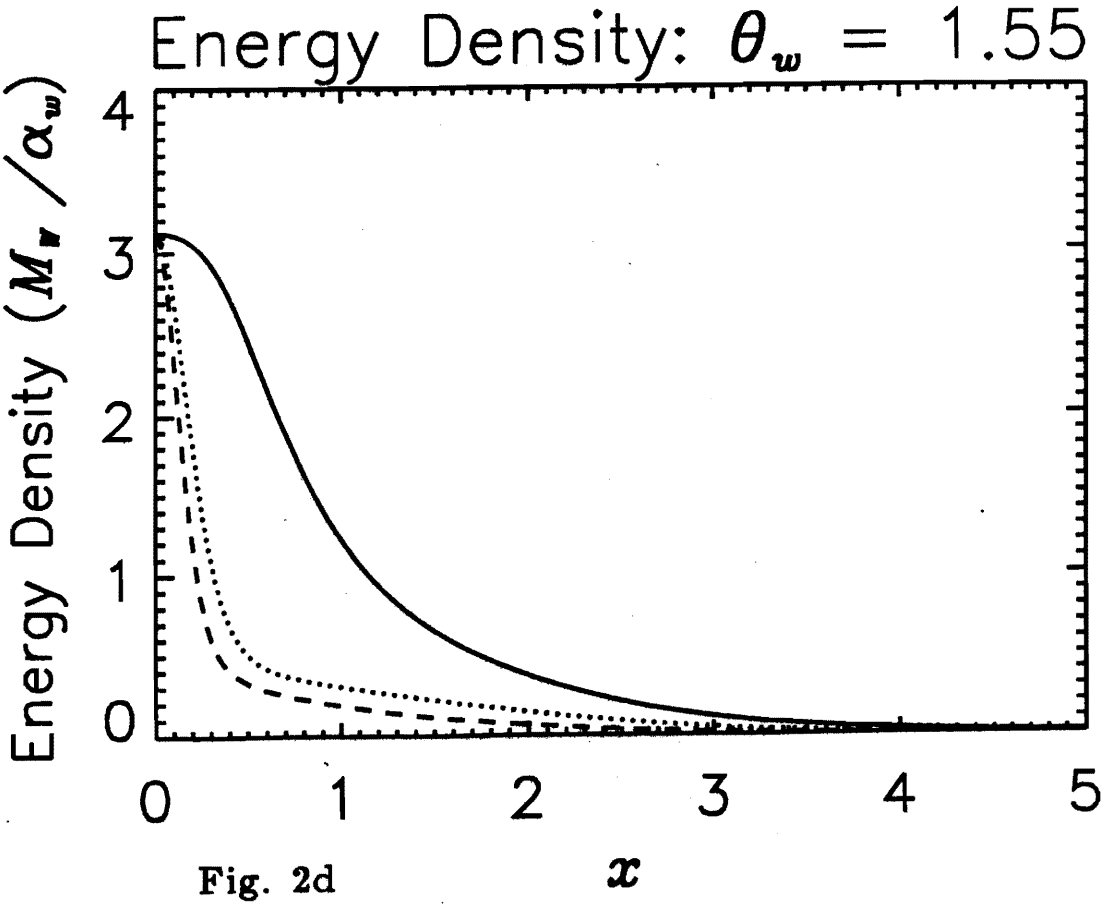
Energy Density: θ_w = 1.55
Energy Density (M_r /α_w)
4
3
2
1
0
0
1
2
3
4
5
x

Fig. 2d

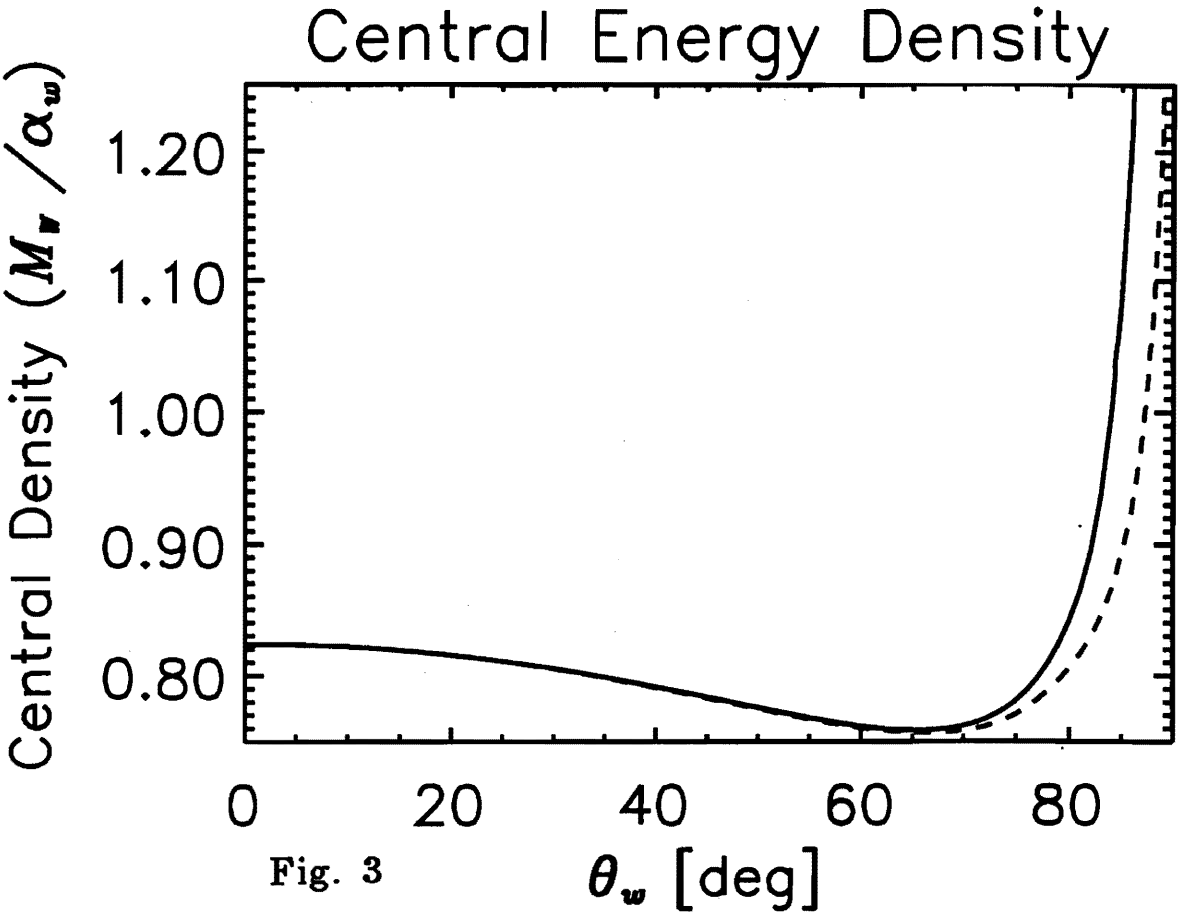
Central Energy Density
Central Density ($M_\bullet / \alpha_w$)
1.20
1.10
1.00
0.90
0.80
0
20
40
60
80
θ_w [deg]

Fig. 3

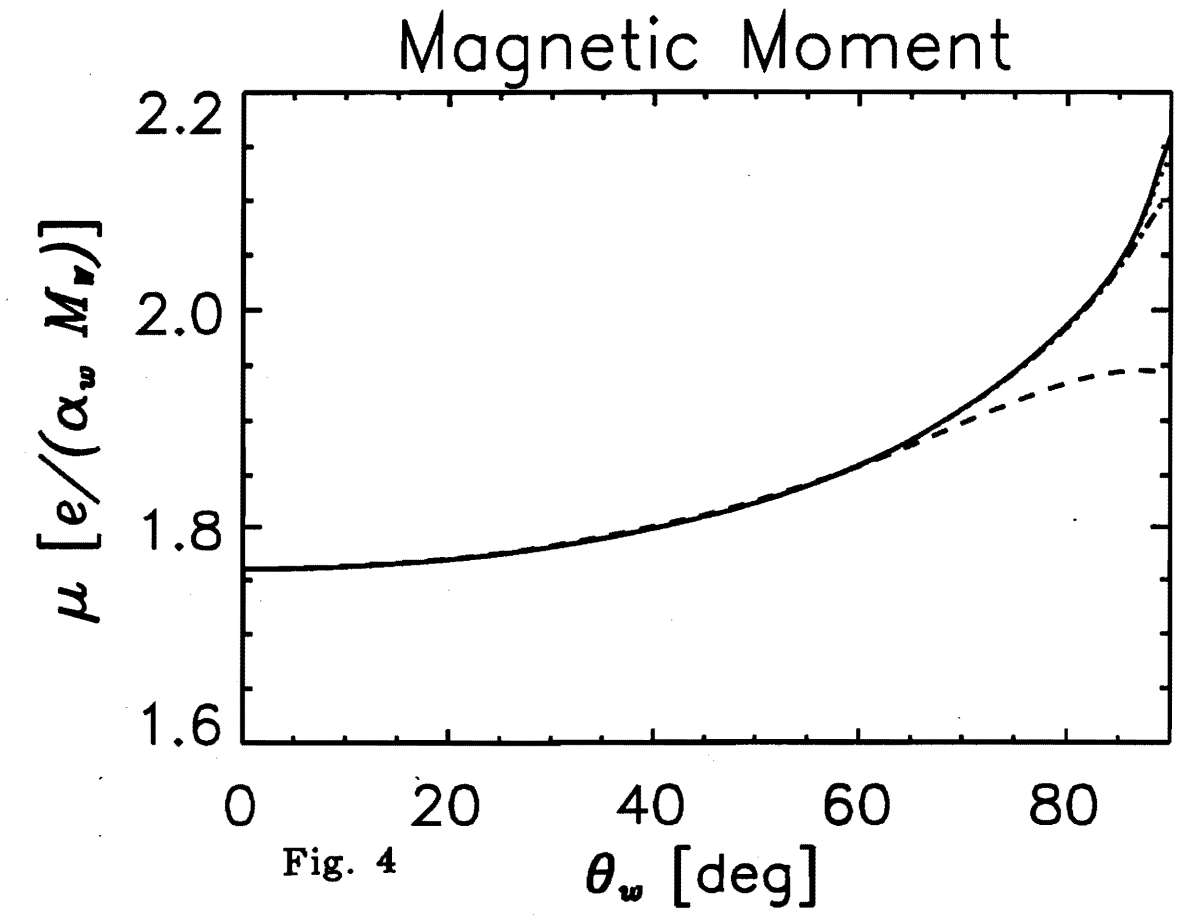
Magnetic Moment
μ [$e/(\alpha_w M_\bullet)$]
2.2
2.0
1.8
1.6
0
20
40
60
80
θ_w [deg]

Fig. 4

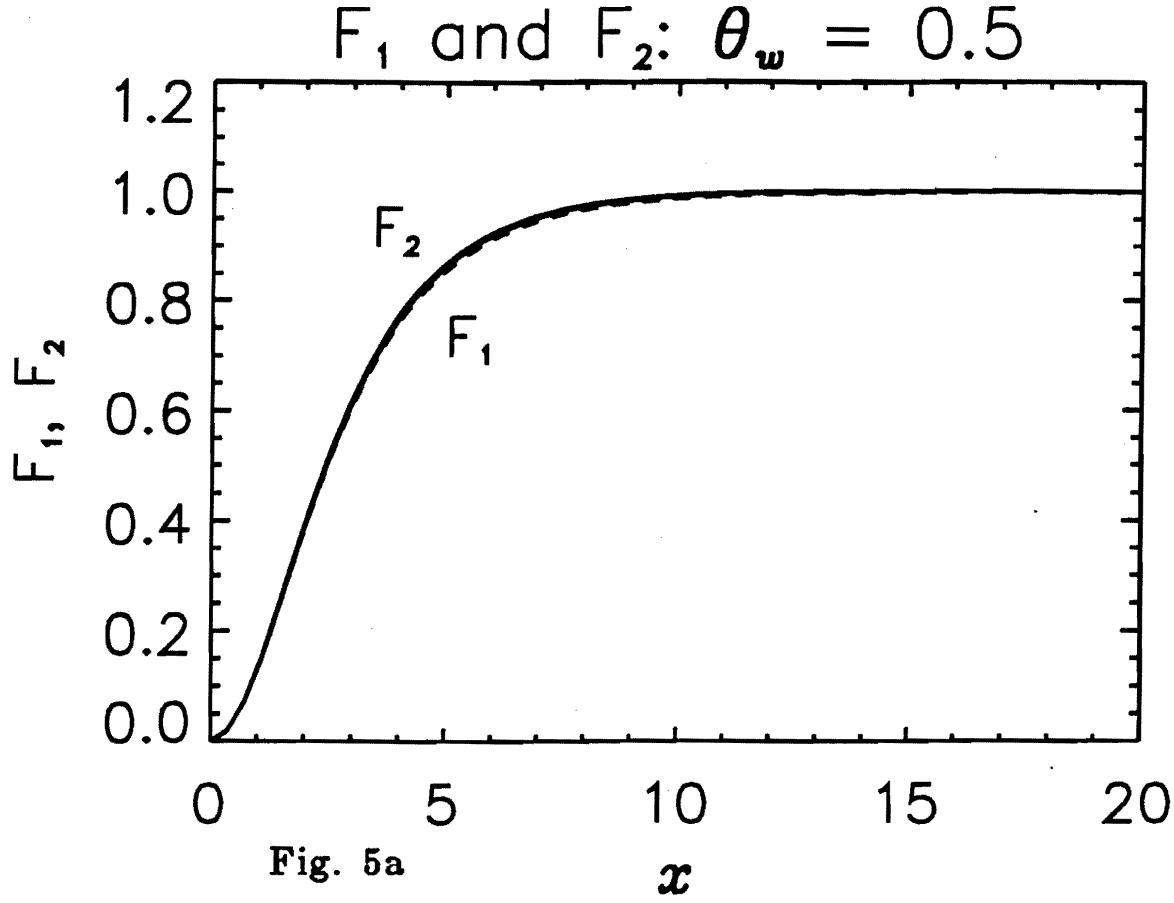
F1 and F2: θw = 0.5
1.2
1.0
0.8
0.6
0.4
0.2
0.0
F1, F2
F2
F1
0
5
10
15
20
x

Fig. 5a

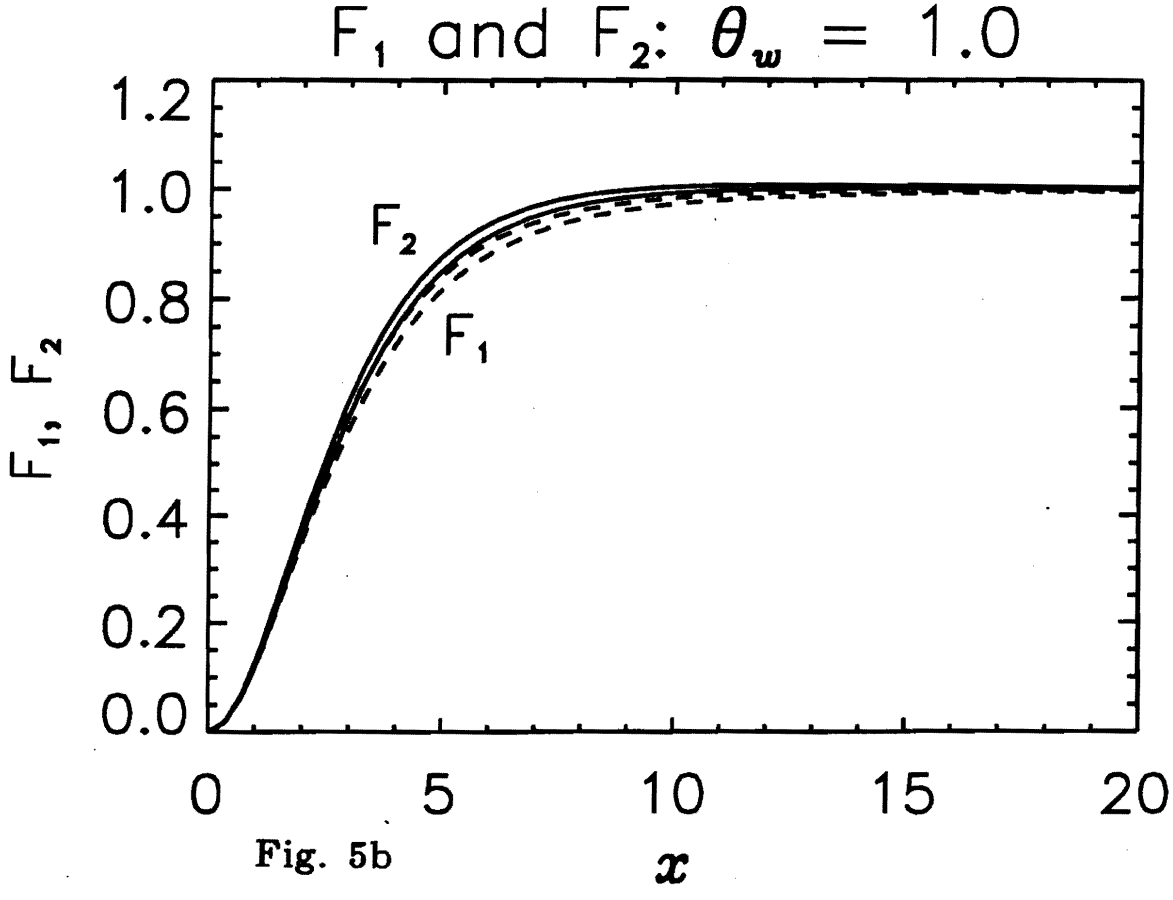
F1 and F2: θw = 1.0
1.2
1.0
0.8
0.6
0.4
0.2
0.0
F1, F2
F2
F1
0
5
10
15
20
x

Fig. 5b

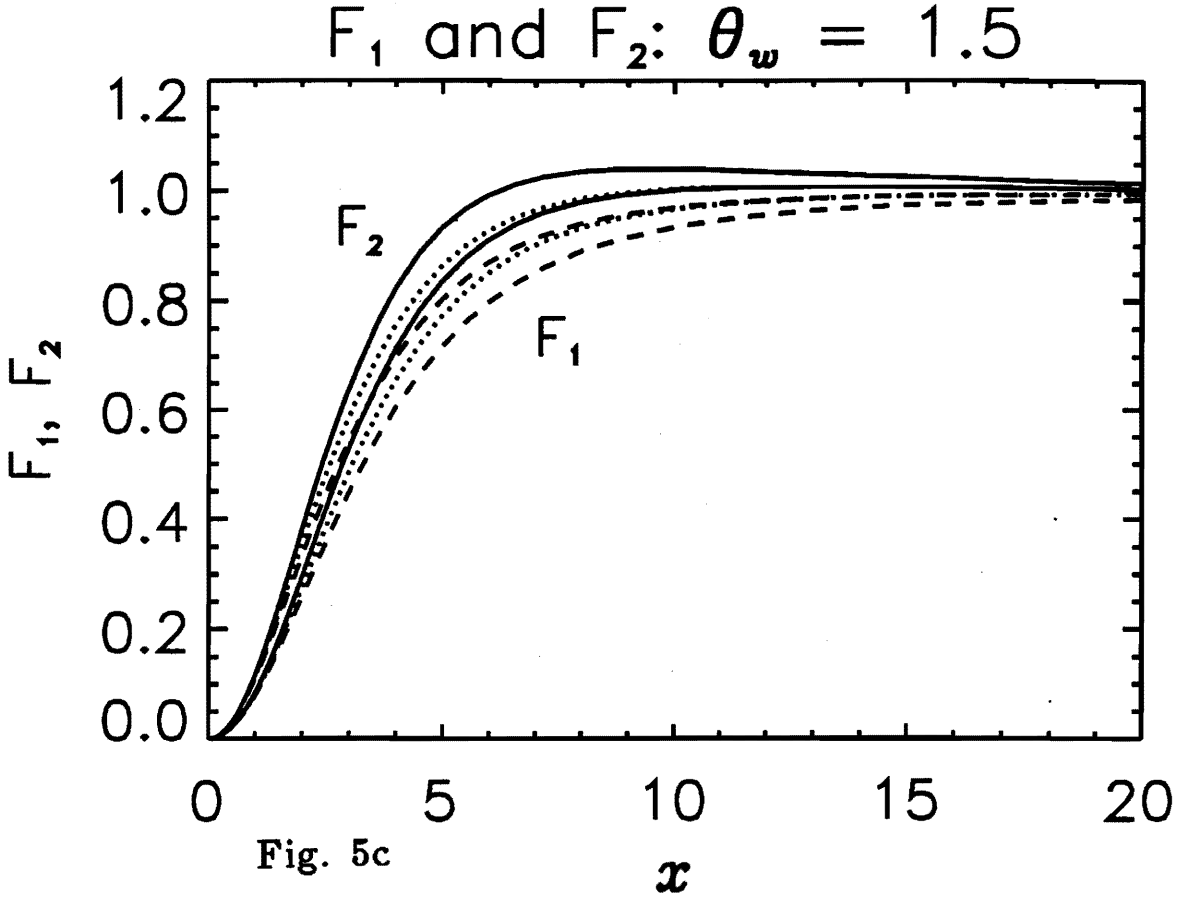
F1 and F2: θw = 1.5
F2
F1
F1, F2
x
0.0
0.2
0.4
0.6
0.8
1.0
1.2
0
5
10
15
20

Fig. 5c

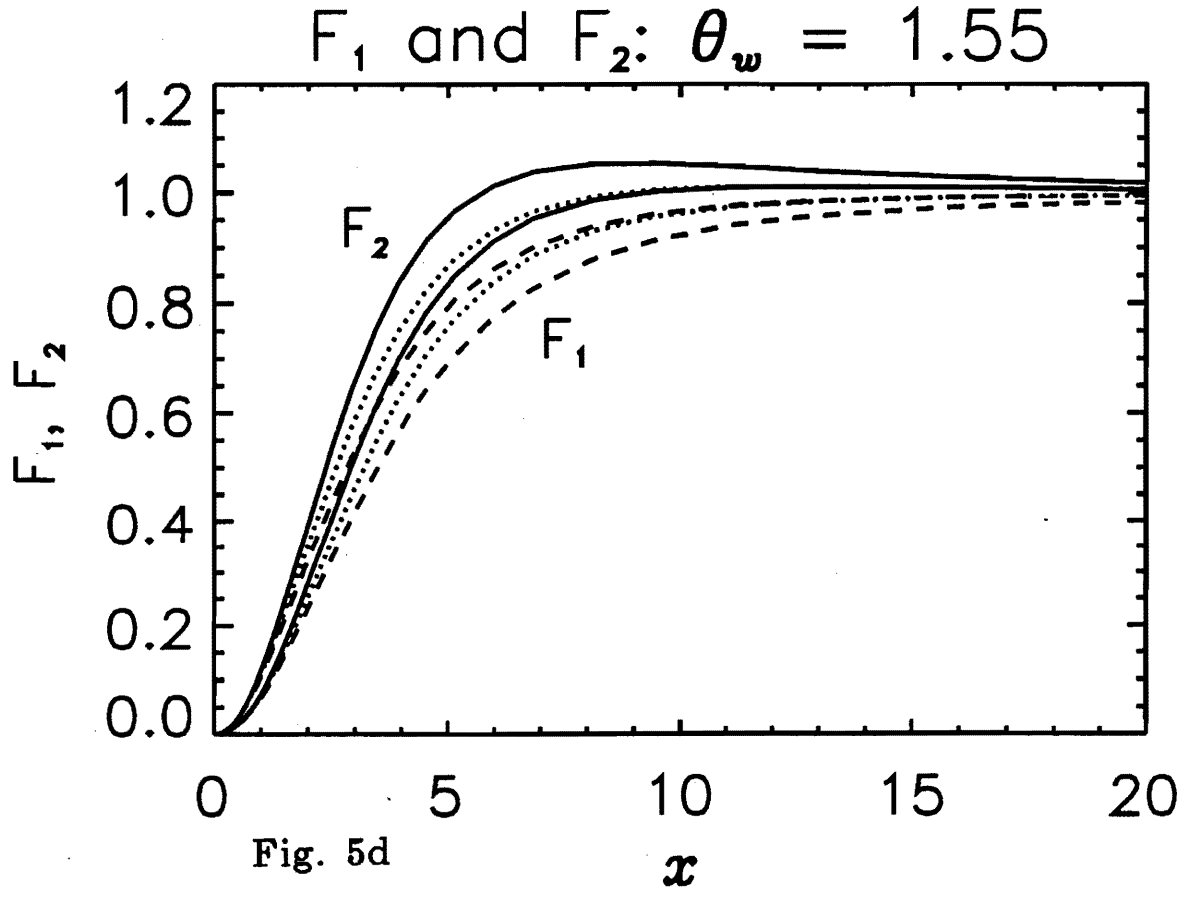
F1 and F2: θw = 1.55
F2
F1
F1, F2
x
0.0
0.2
0.4
0.6
0.8
1.0
1.2
0
5
10
15
20

Fig. 5d

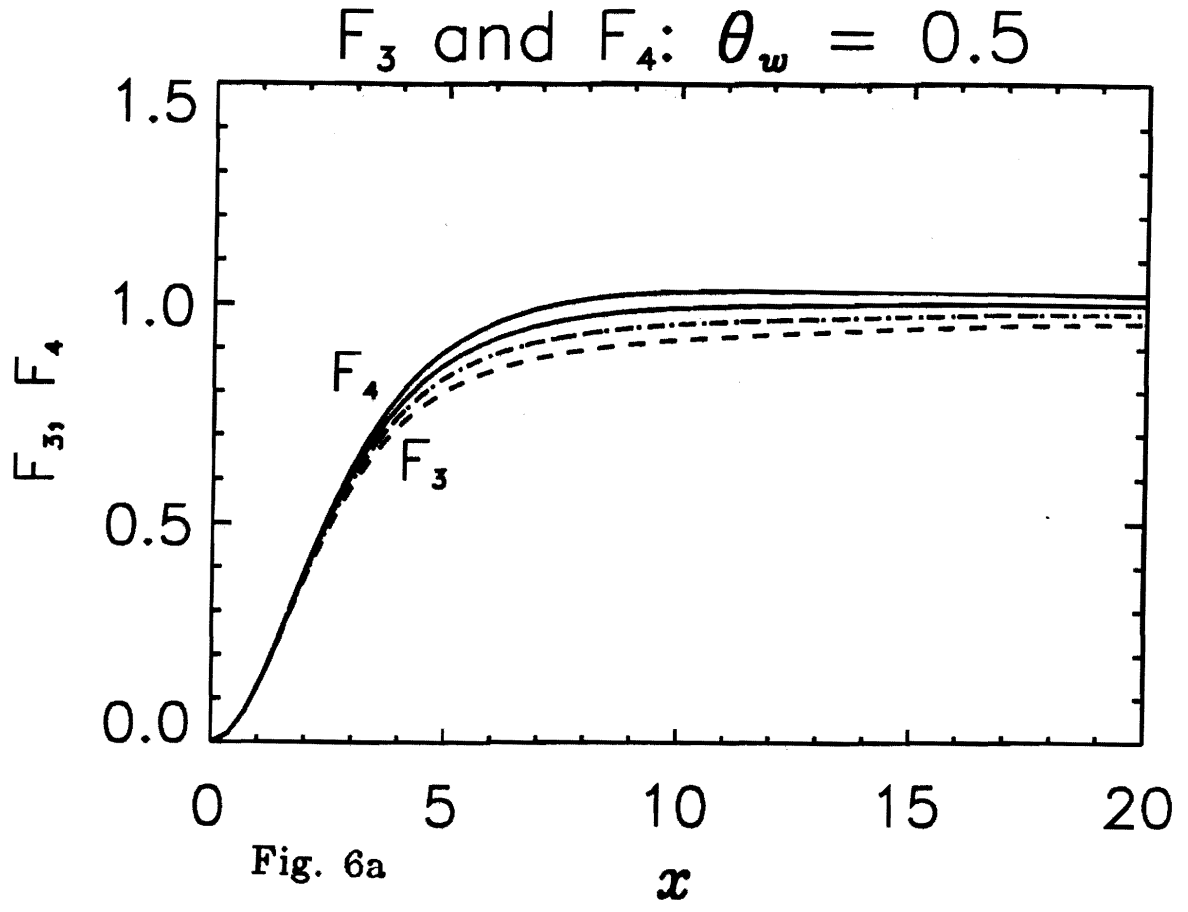
F3 and F4: θw = 0.5
1.5
1.0
0.5
0.0
F3, F4
F4
F3
0
5
10
15
20
x

Fig. 6a

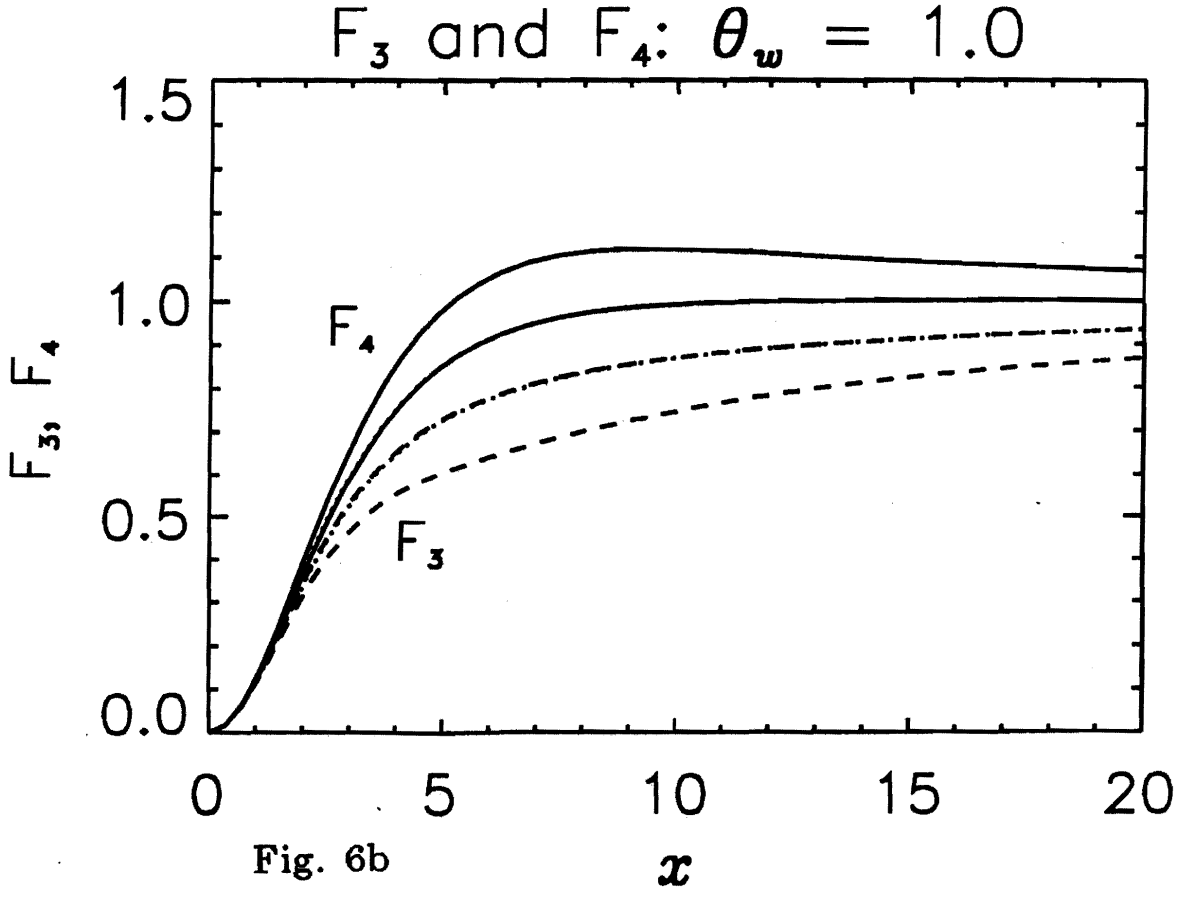
F3 and F4: θw = 1.0
1.5
1.0
0.5
0.0
F3, F4
F4
F3
0
5
10
15
20
x

Fig. 6b

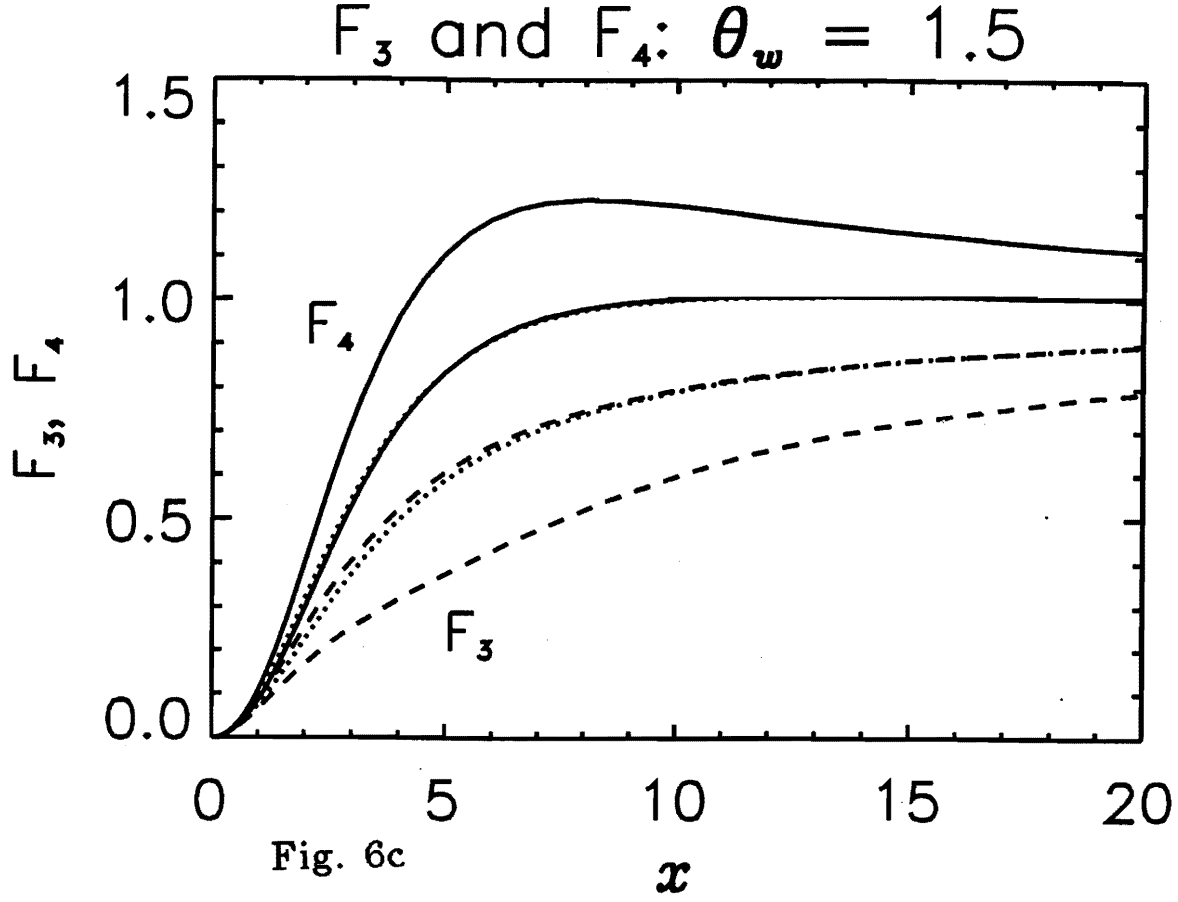
F3 and F4: θw = 1.5
1.5
1.0
0.5
0.0
F3, F4
F4
F3
0
5
10
15
20
x

Fig. 6c

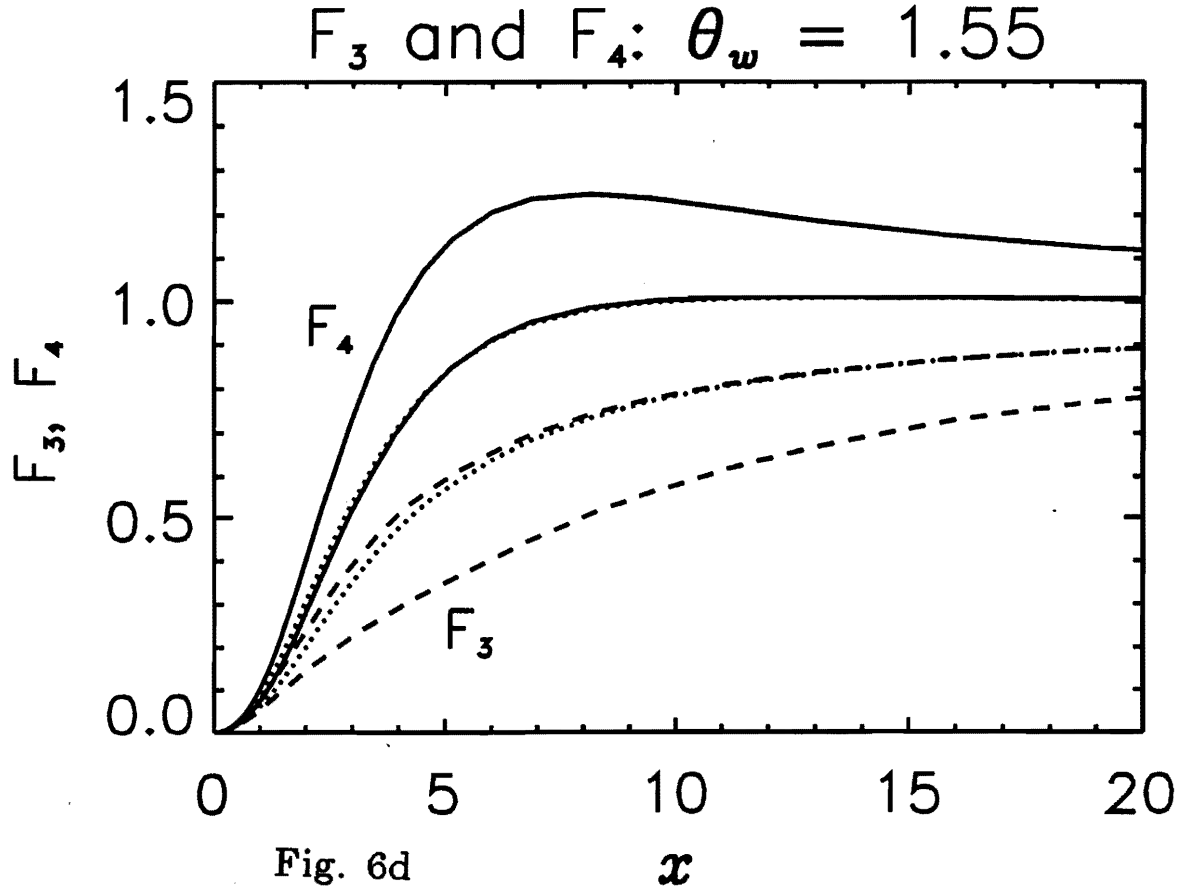
F3 and F4: θw = 1.55
1.5
1.0
0.5
0.0
F3, F4
F4
F3
0
5
10
15
20
x

Fig. 6d

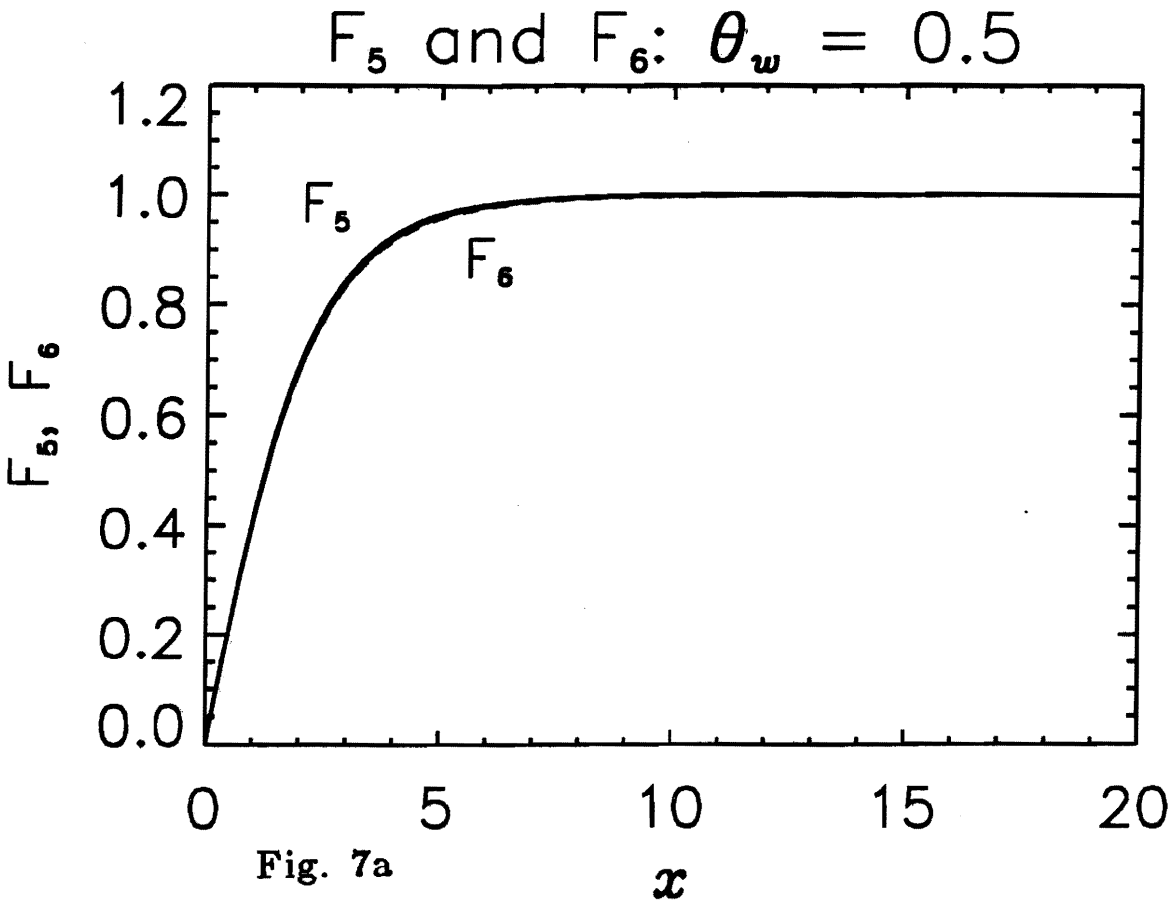
F5 and F6: θw = 0.5
1.2
1.0
0.8
0.6
0.4
0.2
0.0
F5, F6
F5
F6
0
5
10
15
20
x

Fig. 7a

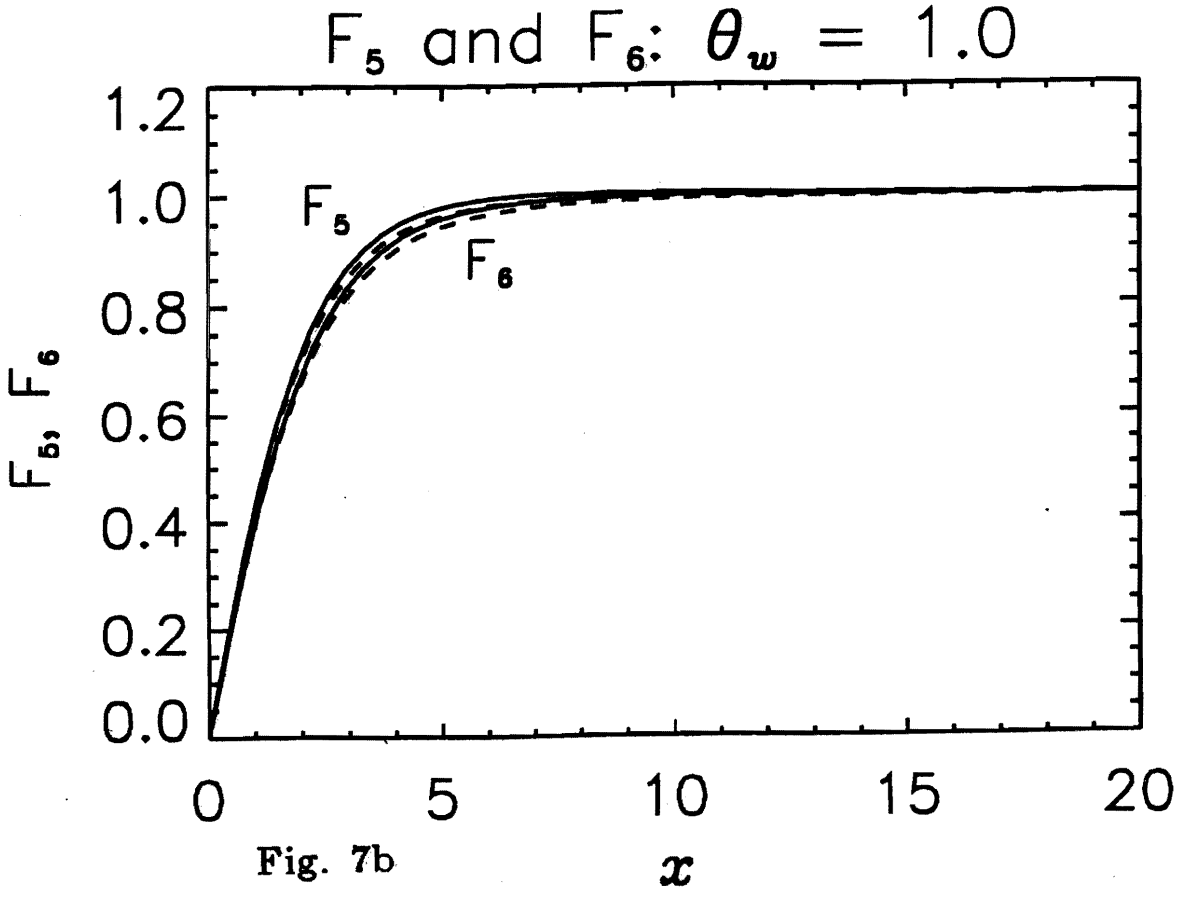
F5 and F6: θw = 1.0
1.2
1.0
0.8
0.6
0.4
0.2
0.0
F5, F6
F5
F6
0
5
10
15
20
x

Fig. 7b

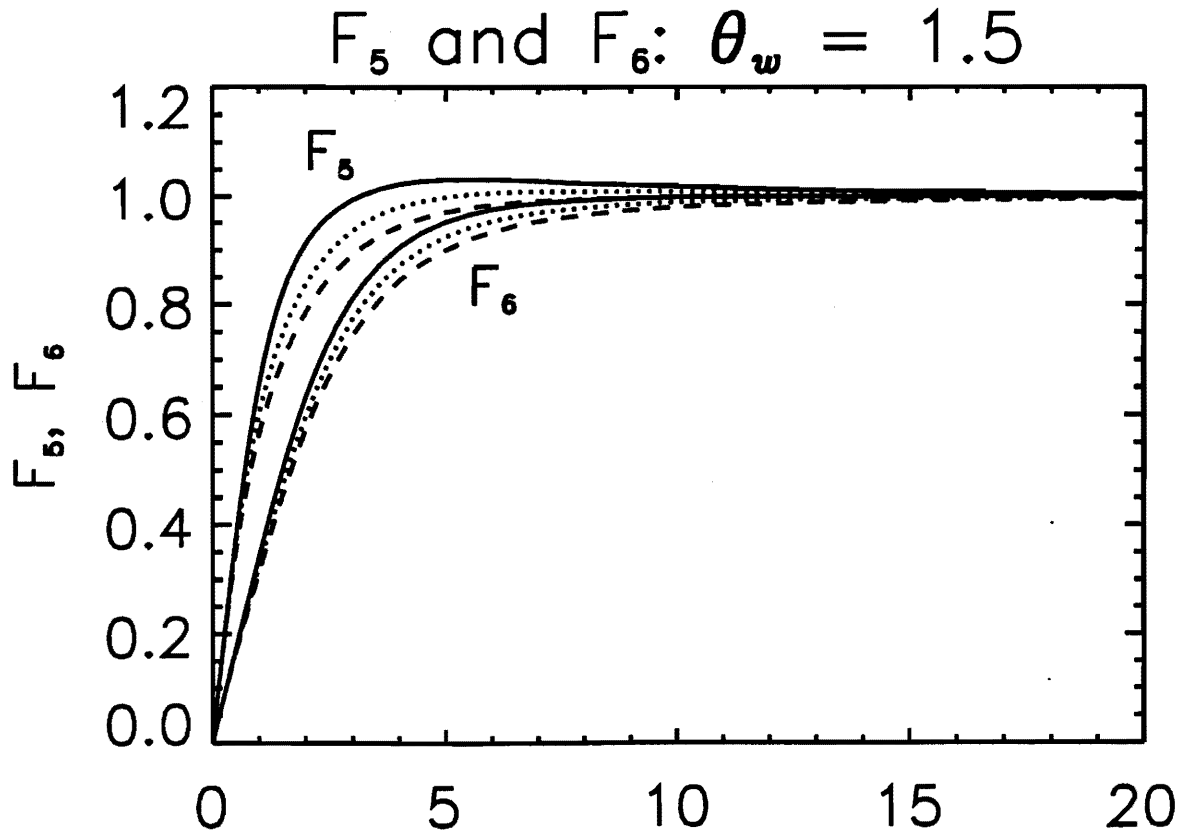
F5 and F6: θw = 1.5
F5
F6
F5, F6
1.2
1.0
0.8
0.6
0.4
0.2
0.0
0
5
10
15
20
x

Fig. 7c

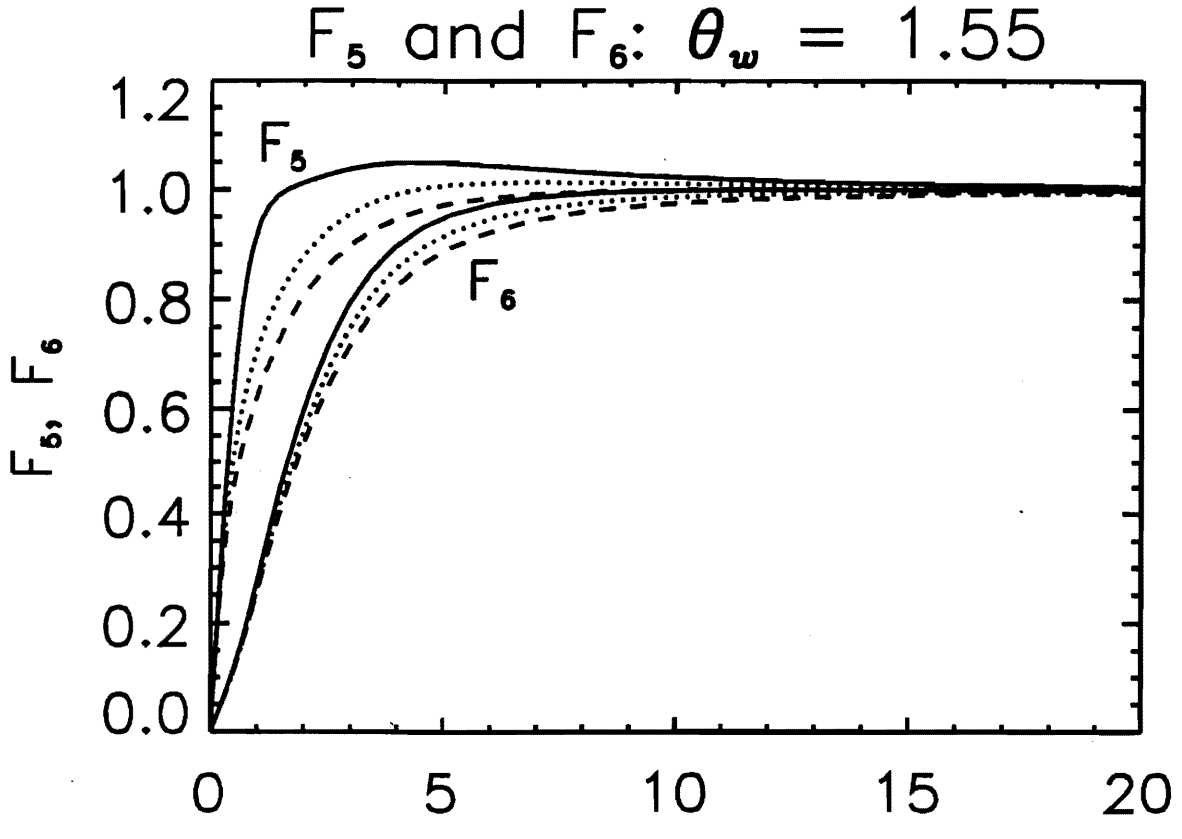
F5 and F6: θw = 1.55
F5
F6
F5, F6
1.2
1.0
0.8
0.6
0.4
0.2
0.0
0
5
10
15
20
x

Fig. 7d

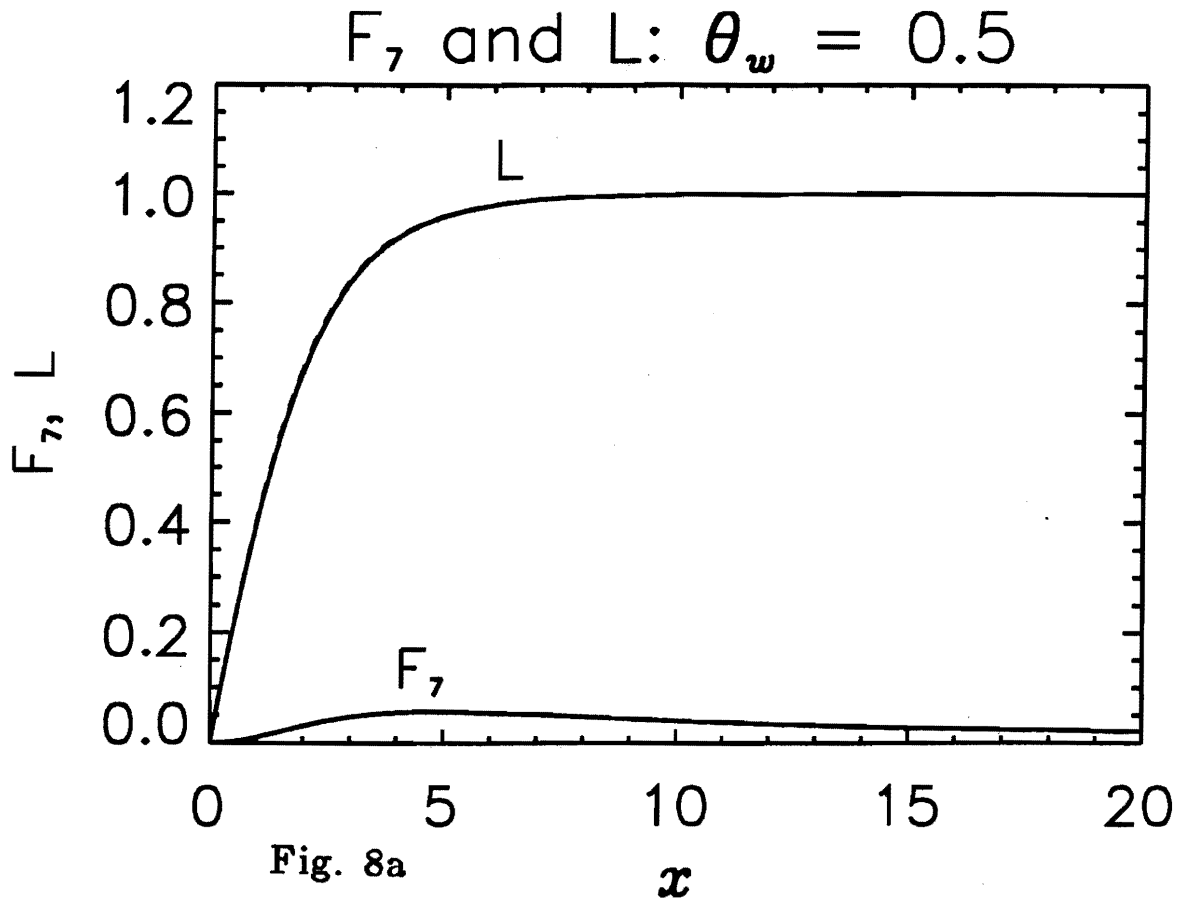
F7 and L: θw = 0.5
1.2
1.0
0.8
0.6
0.4
0.2
0.0
F7, L
L
F7
0
5
10
15
20
x

Fig. 8a

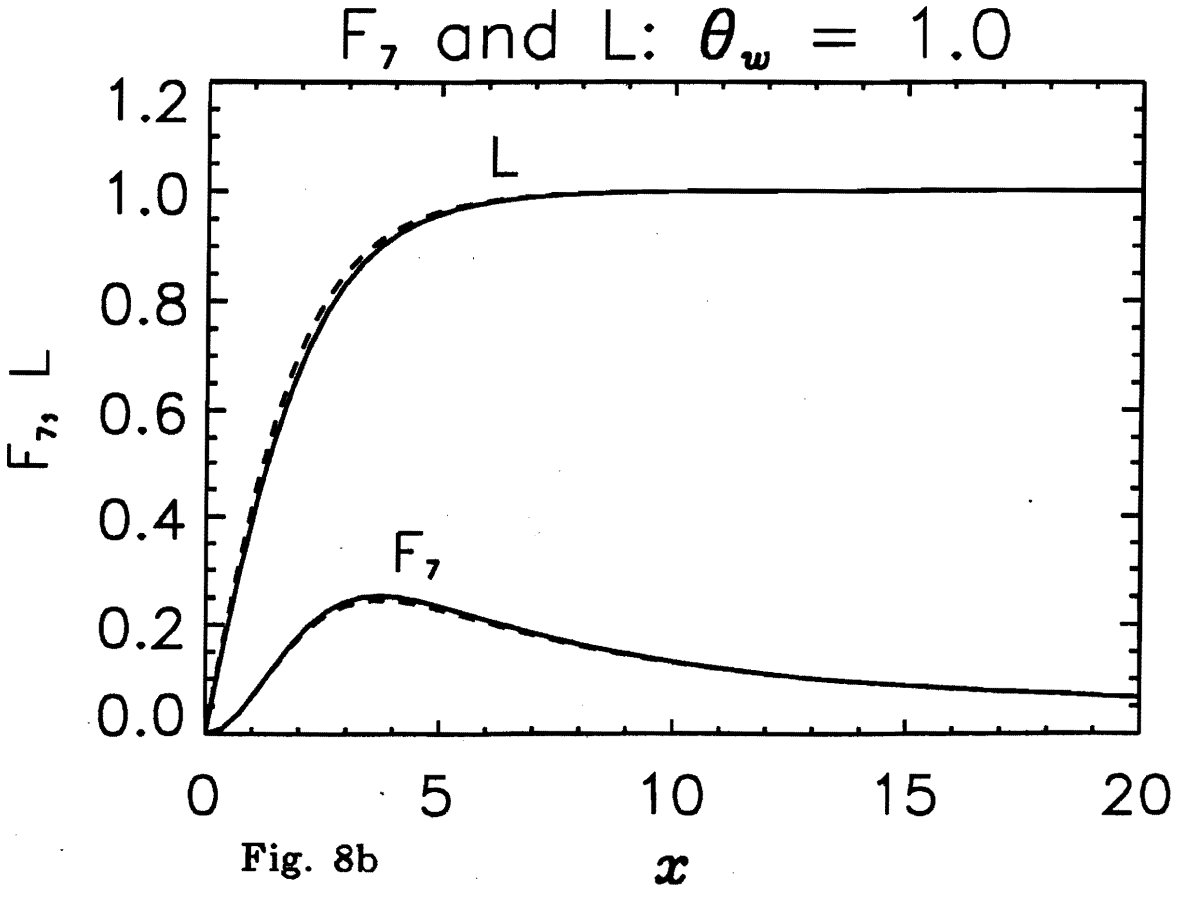
F7 and L: θw = 1.0
1.2
1.0
0.8
0.6
0.4
0.2
0.0
F7, L
L
F7
0
5
10
15
20
x

Fig. 8b

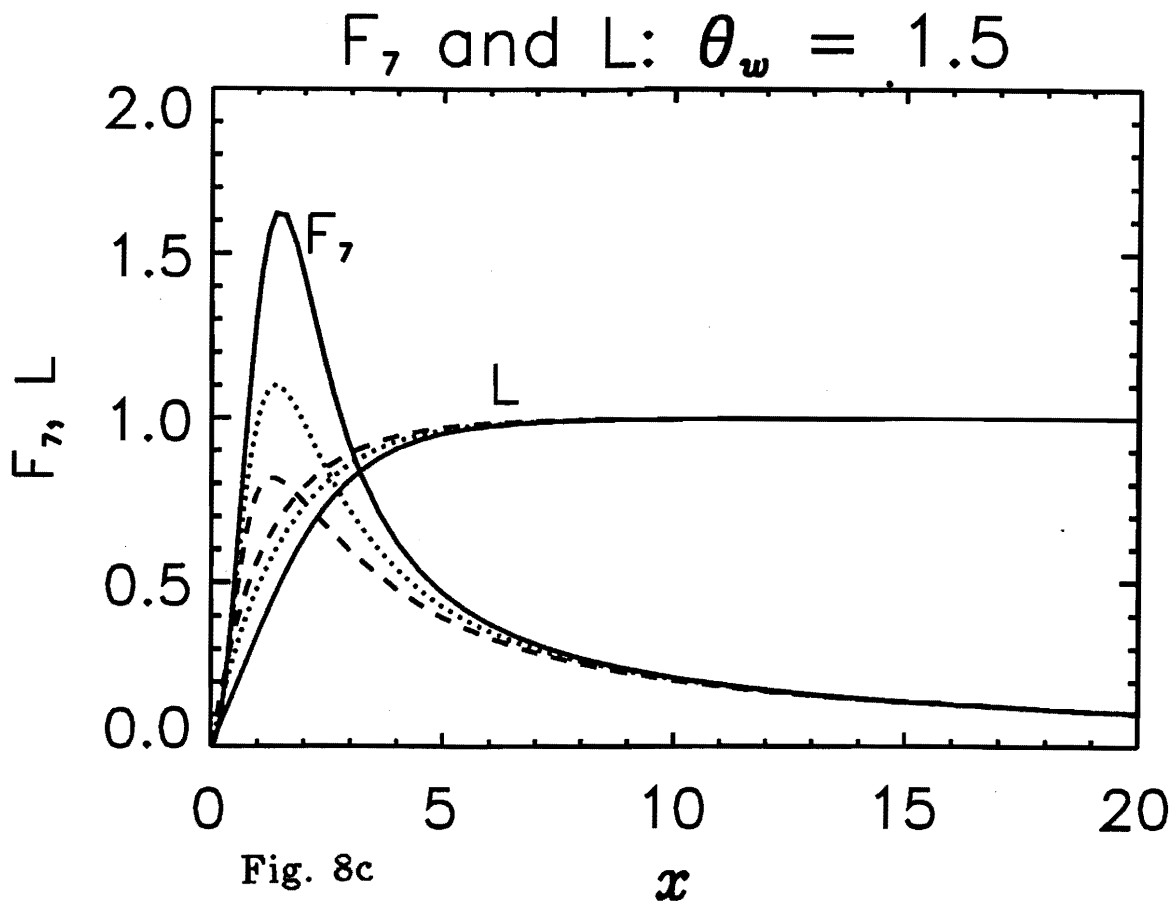
F7 and L: θw = 1.5
2.0
1.5
1.0
0.5
0.0
F7, L
F7
L
0
5
10
15
20
x

Fig. 8c

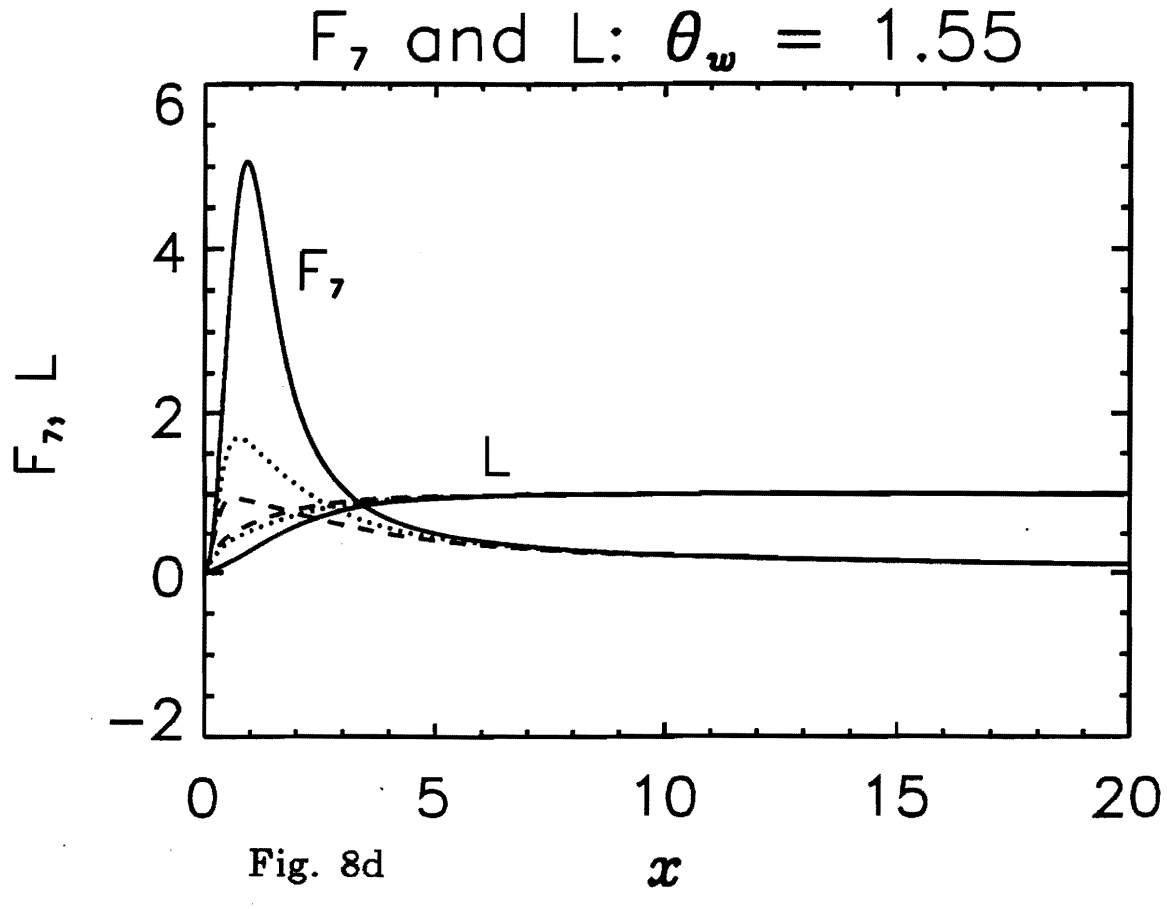
F7 and L: θw = 1.55
6
4
2
0
−2
F7, L
F7
L
0
5
10
15
20
x

Fig. 8d

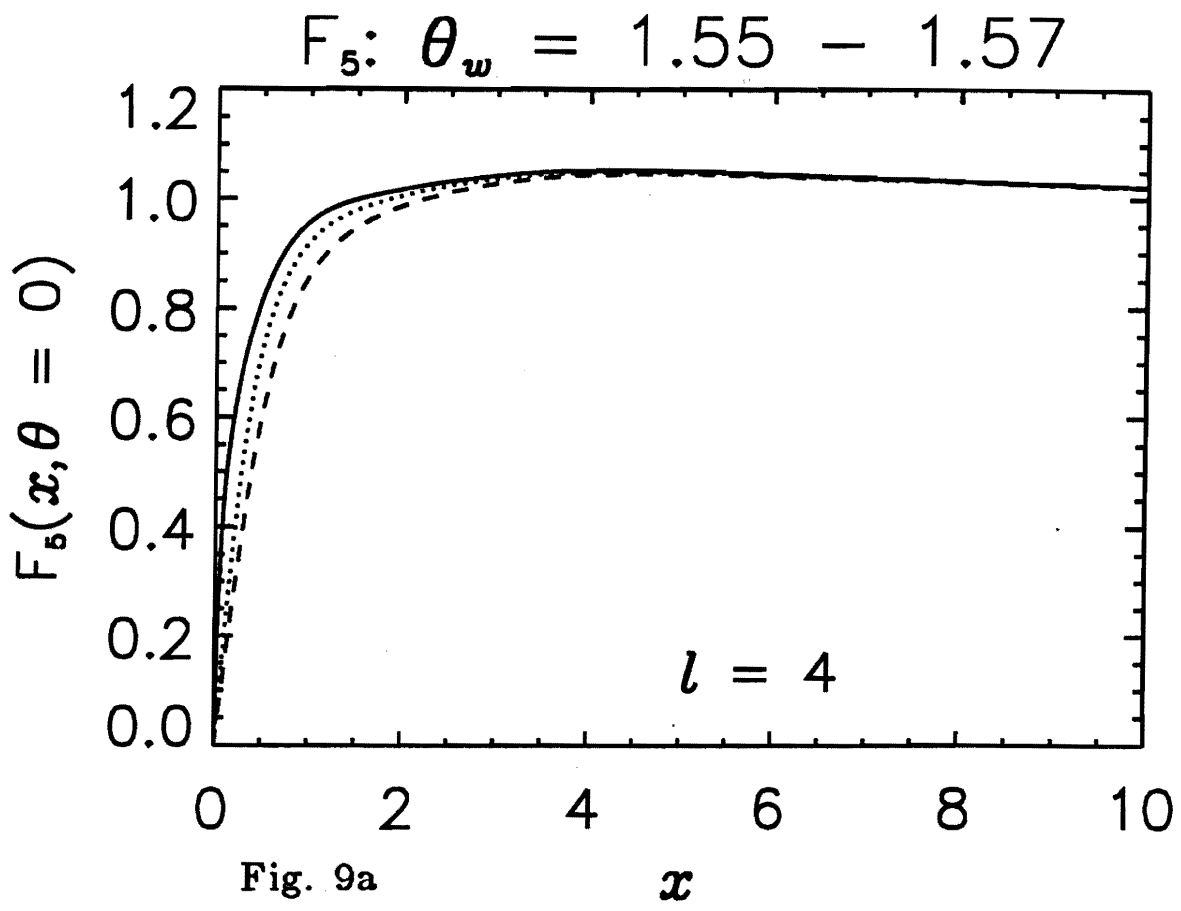
F5: θw = 1.55 − 1.57
F5(x,θ = 0)
1.2
1.0
0.8
0.6
0.4
0.2
0.0
0
2
4
6
8
10
x
l = 4

Fig. 9a

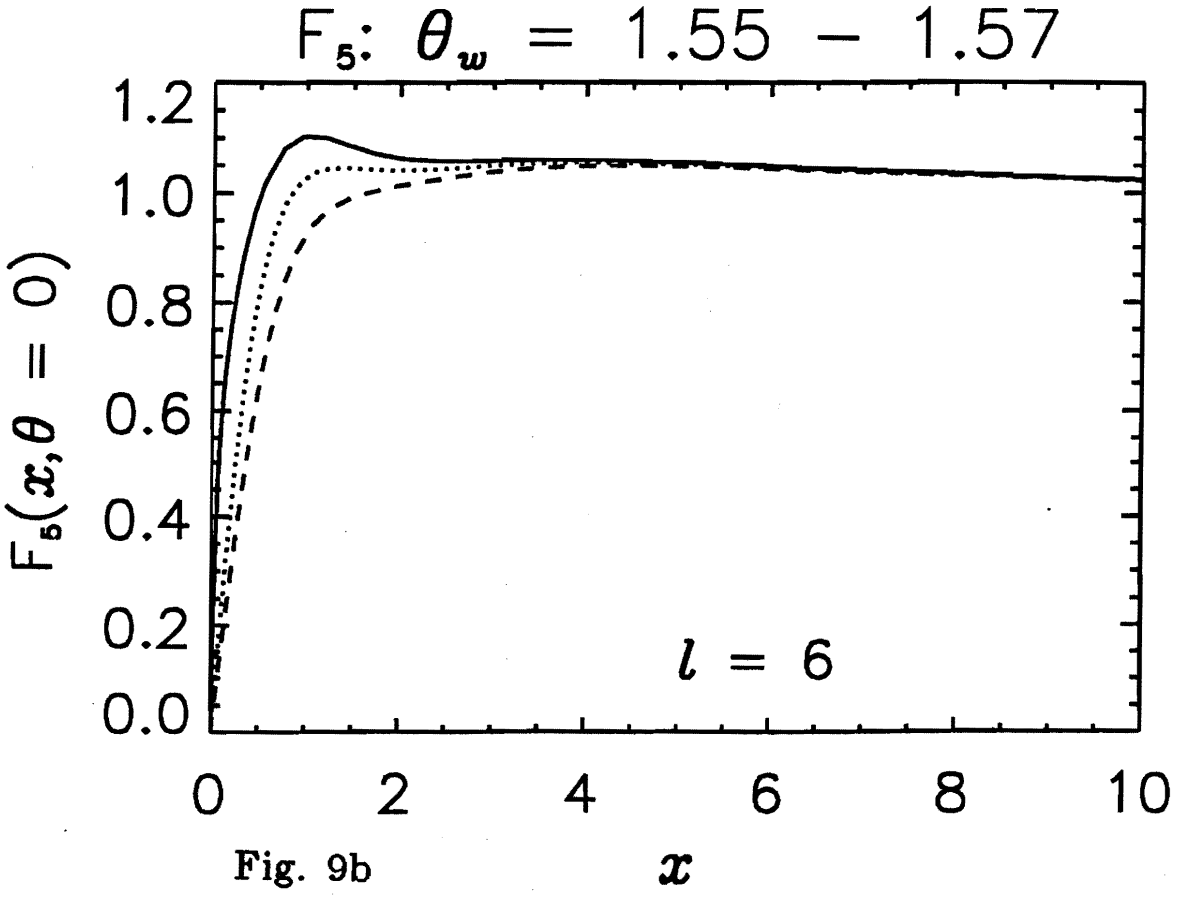
F5: θw = 1.55 − 1.57
F5(x,θ = 0)
1.2
1.0
0.8
0.6
0.4
0.2
0.0
0
2
4
6
8
10
x
l = 6

Fig. 9b

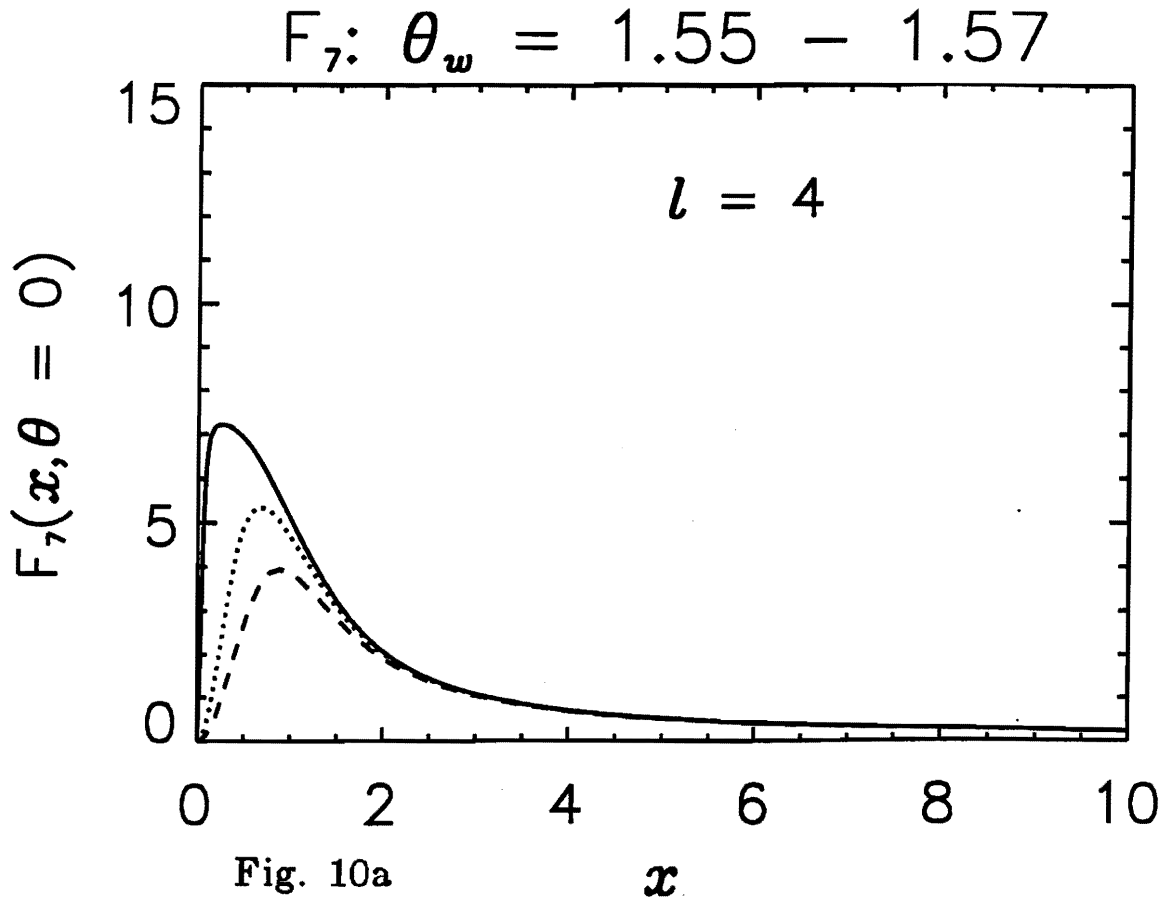

Fig. 10a

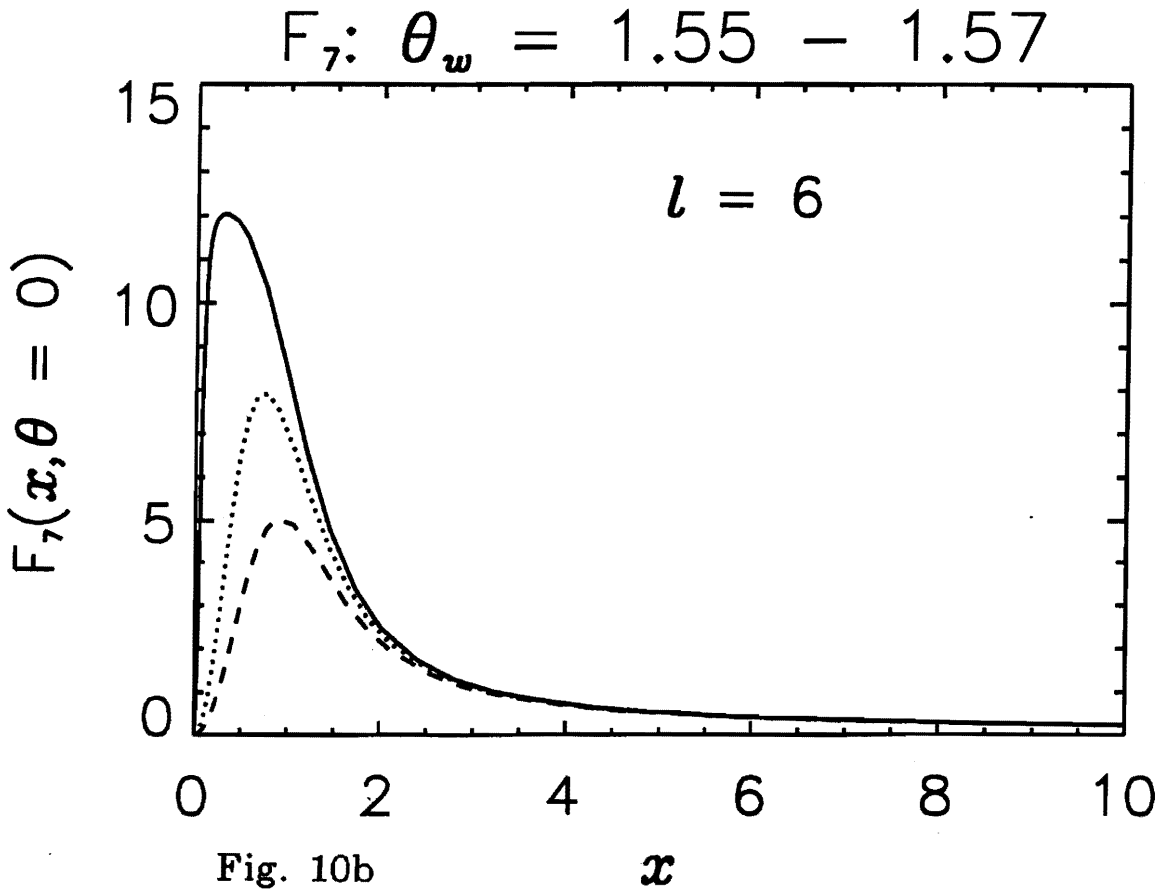

Fig. 10b

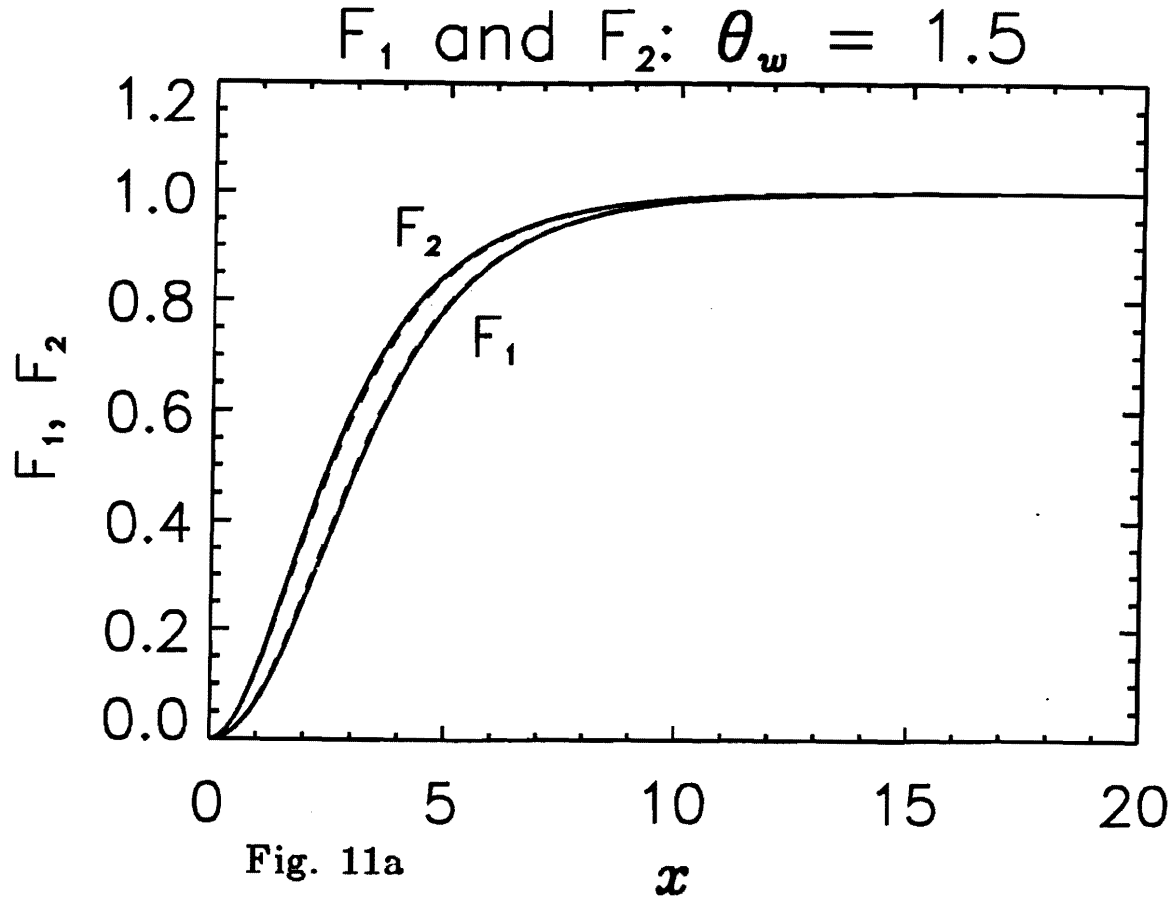

Fig. 11a

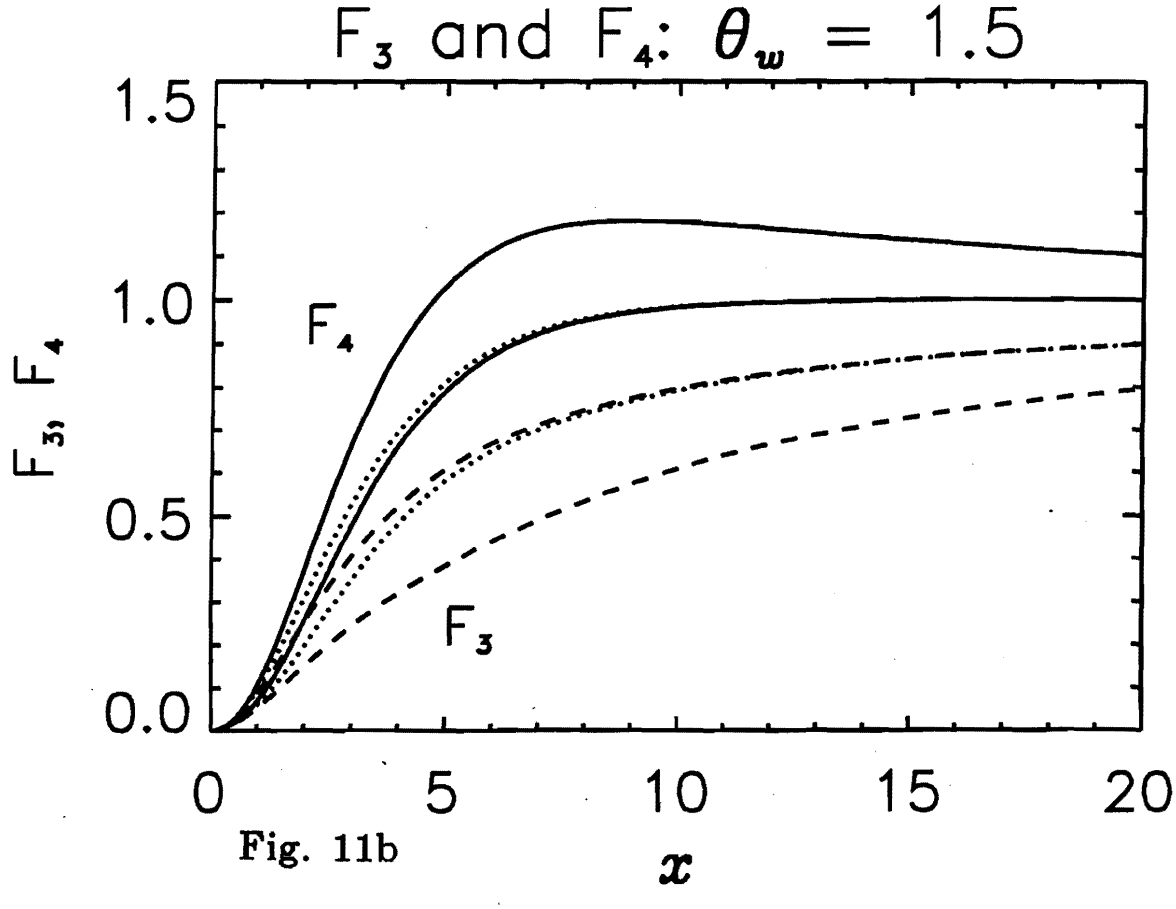

Fig. 11b

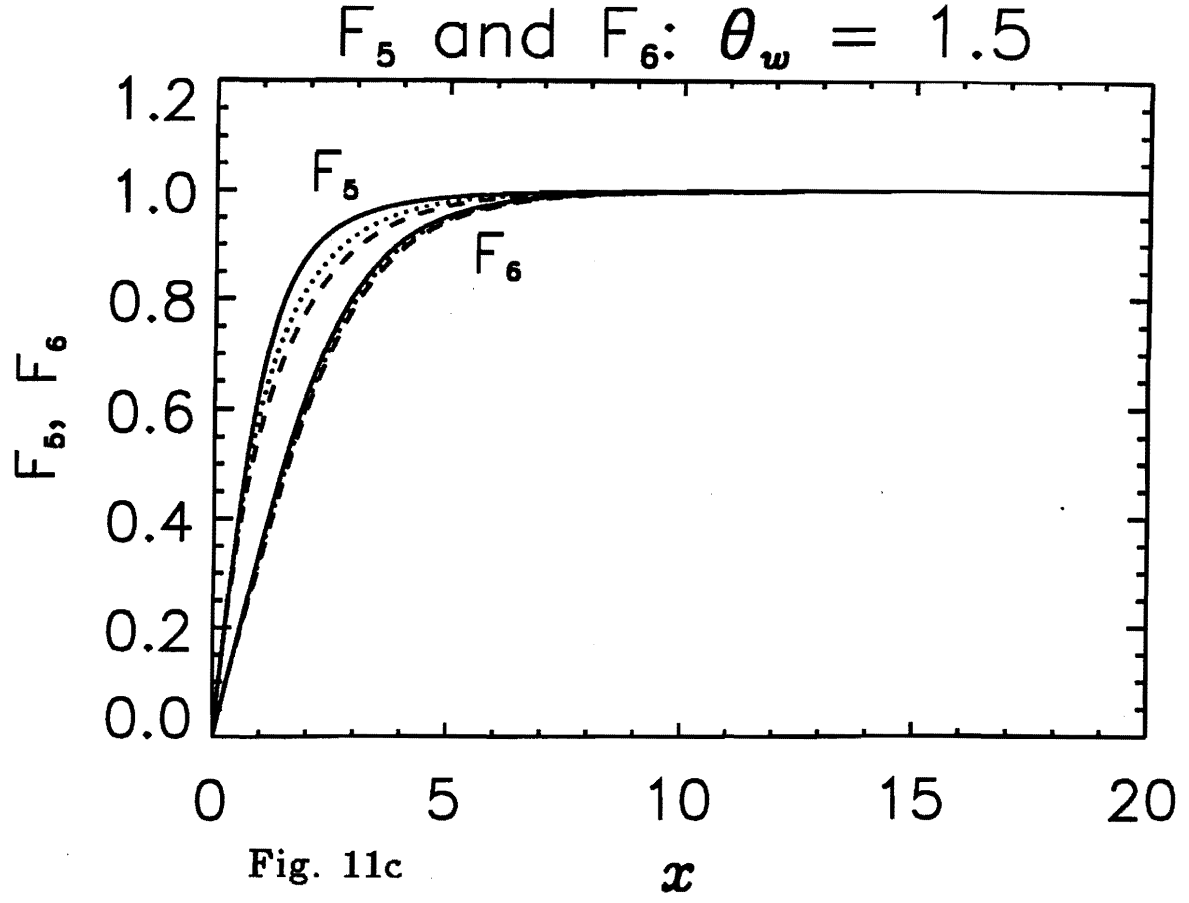

Fig. 11c

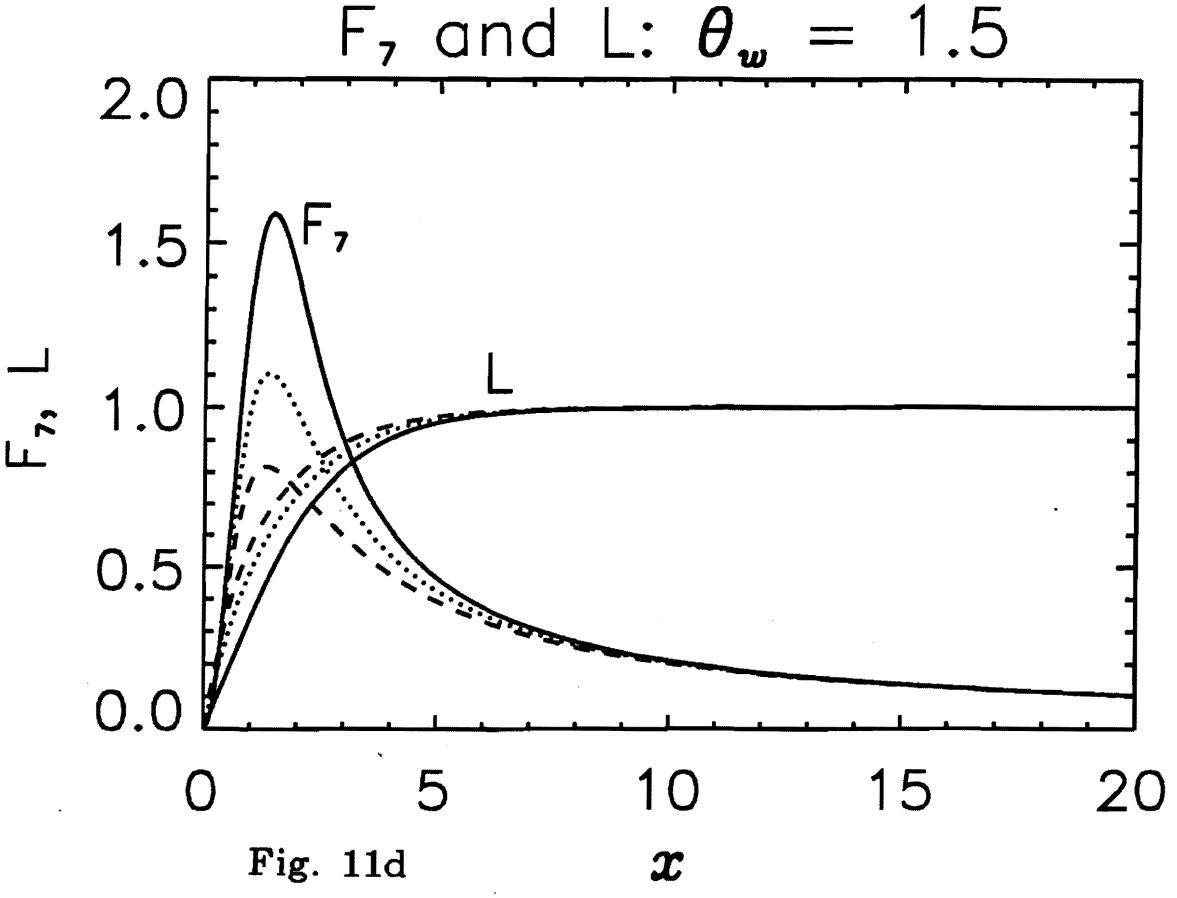

Fig. 11d

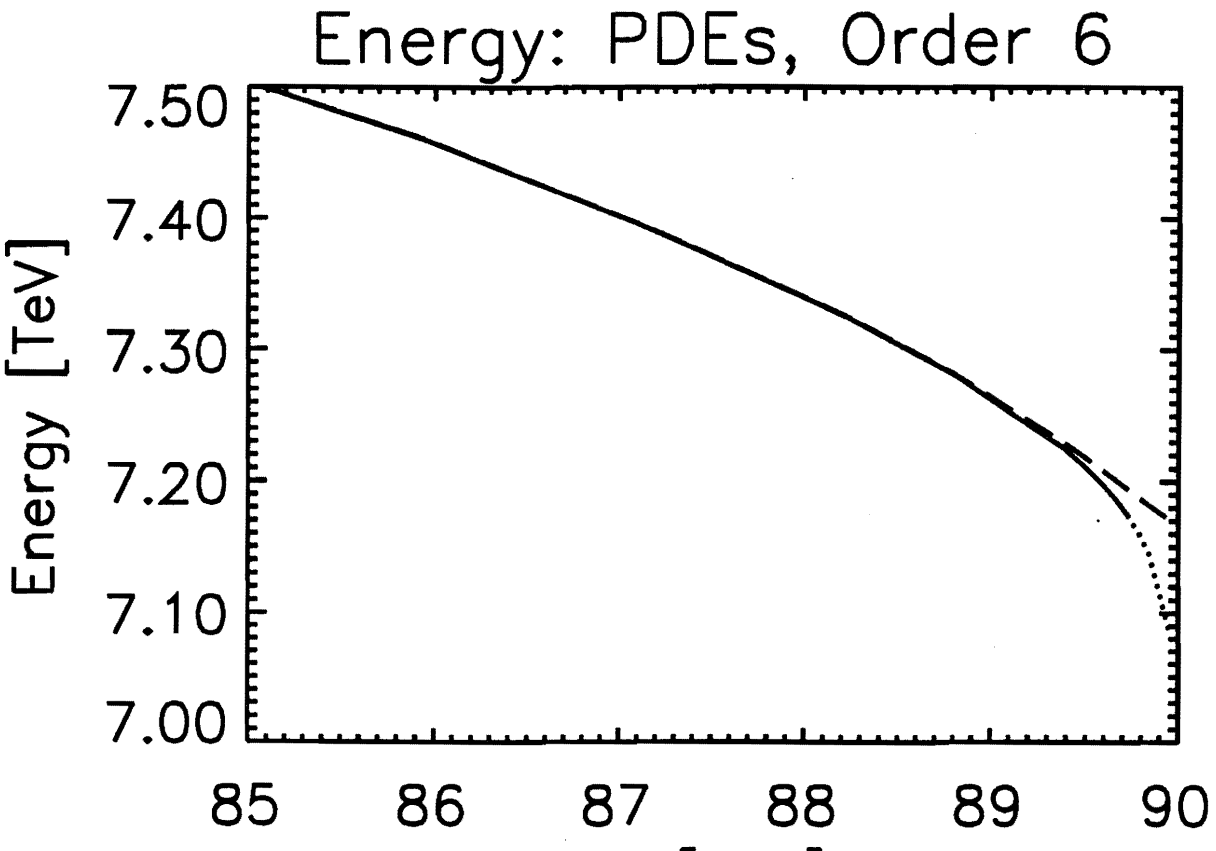
Energy: PDEs, Order 6
7.50
7.40
7.30
7.20
7.10
7.00
Energy [TeV]
85
86
87
88
89
90
θ_w [deg]

Fig. 12

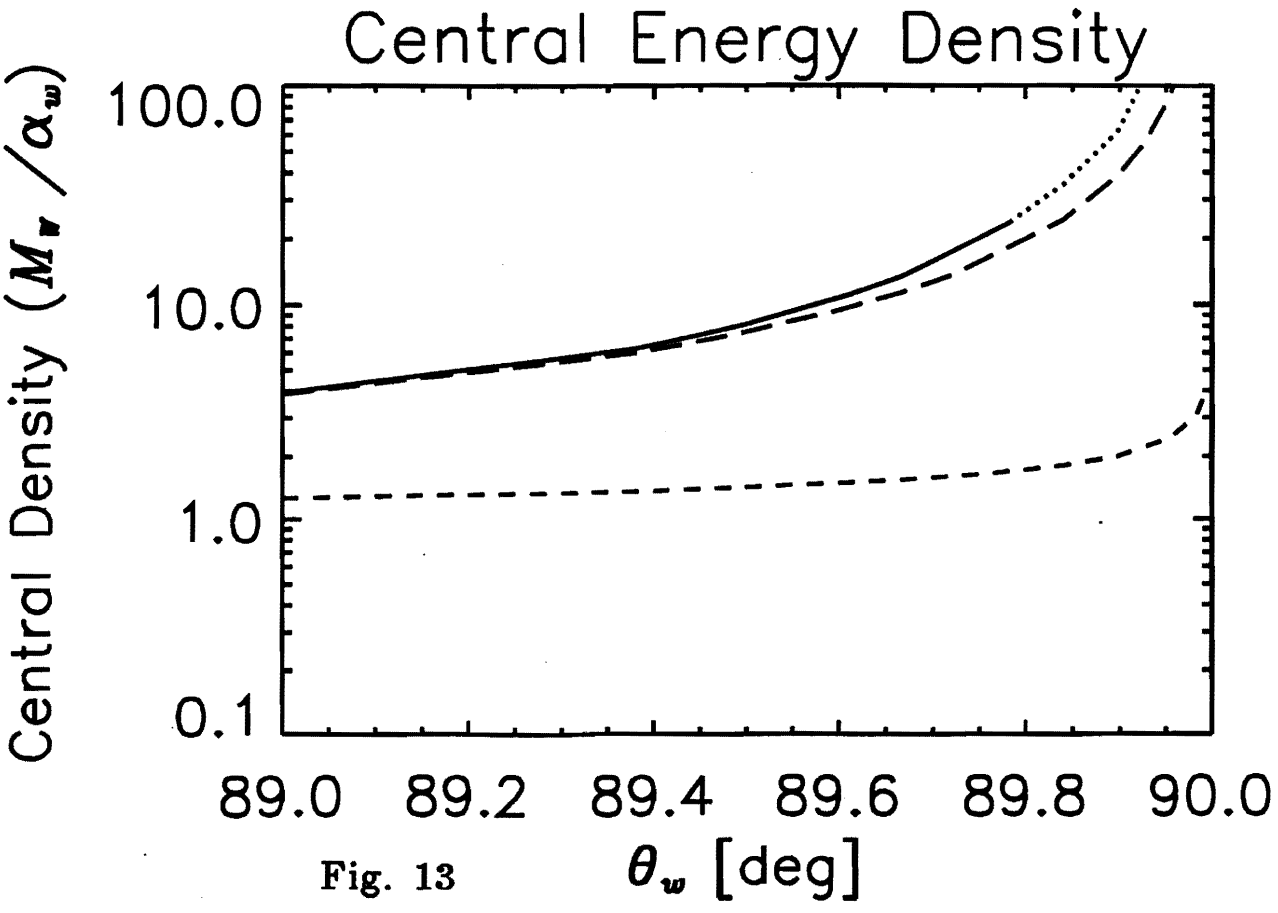
Central Energy Density
100.0
10.0
1.0
0.1
Central Density (M_w/α_w)
89.0
89.2
89.4
89.6
89.8
90.0
θ_w [deg]

Fig. 13

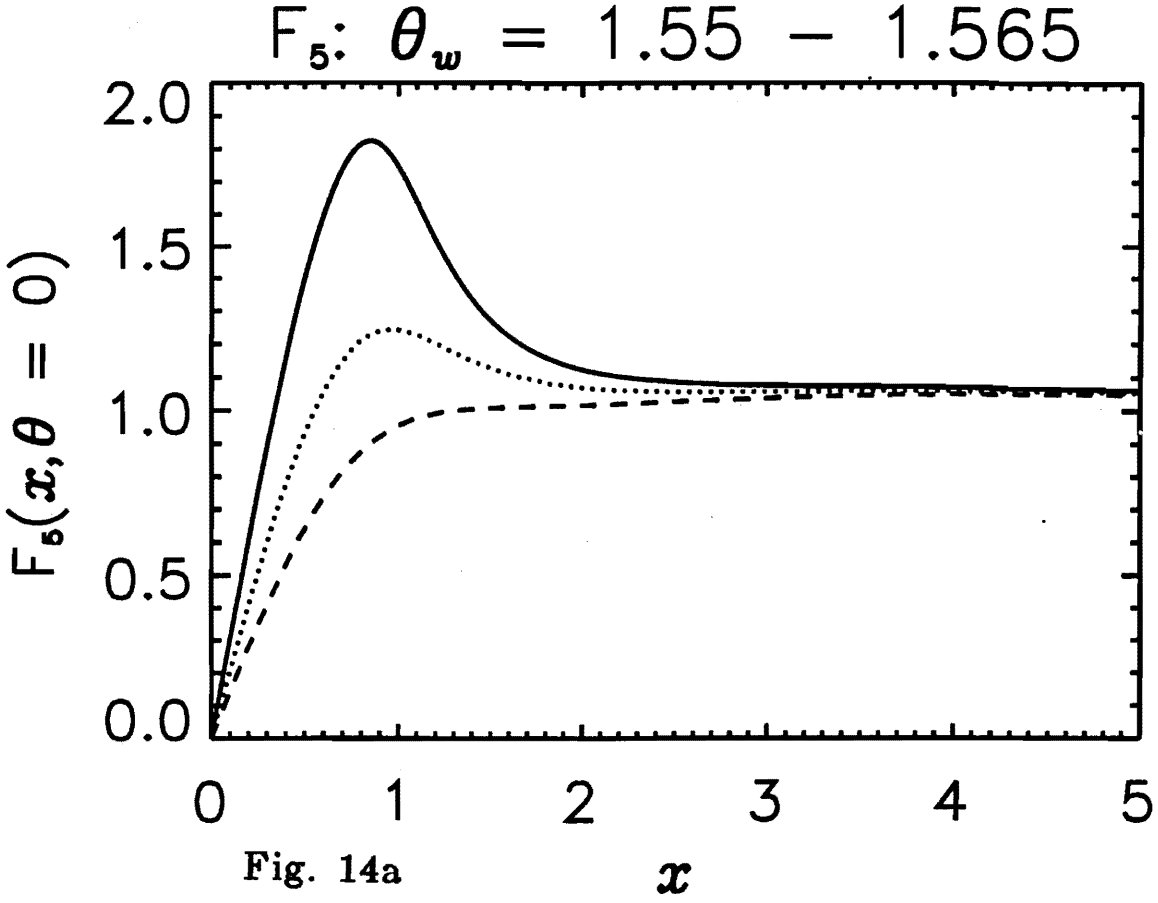

Fig. 14a

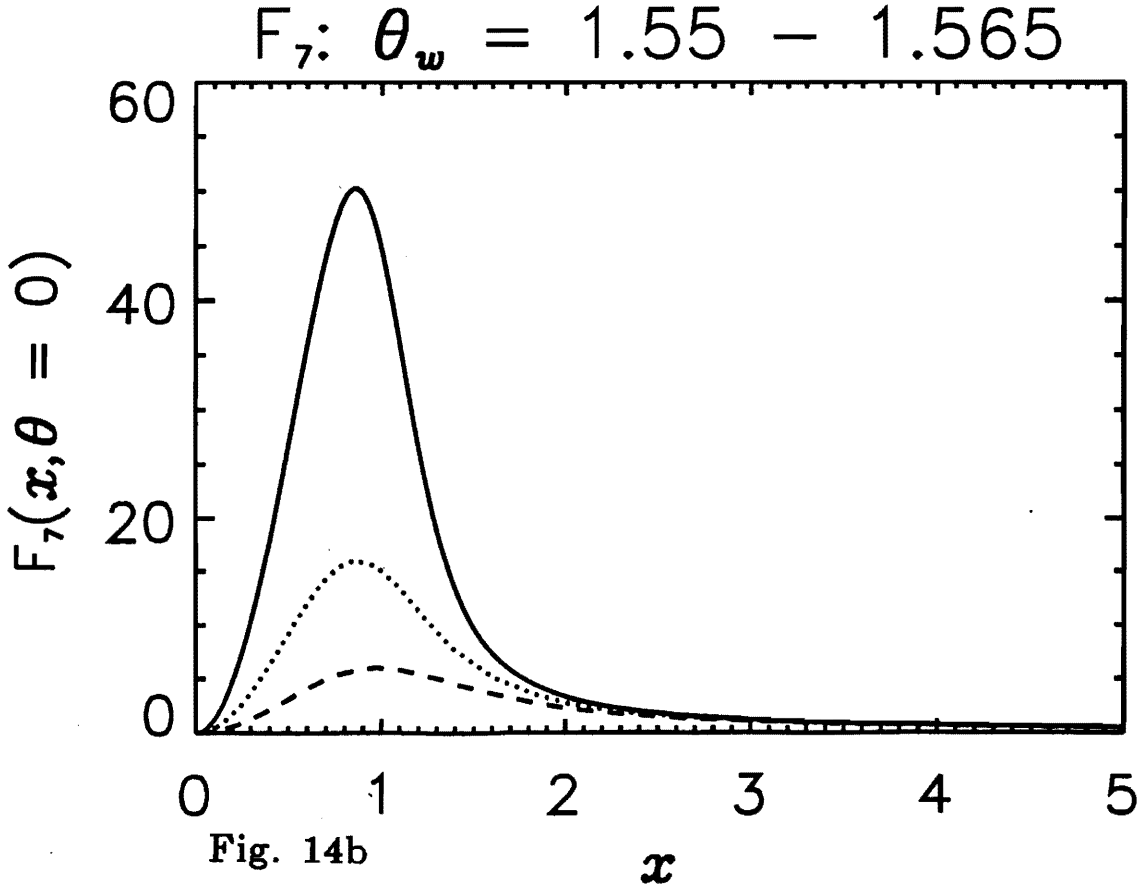

Fig. 14b

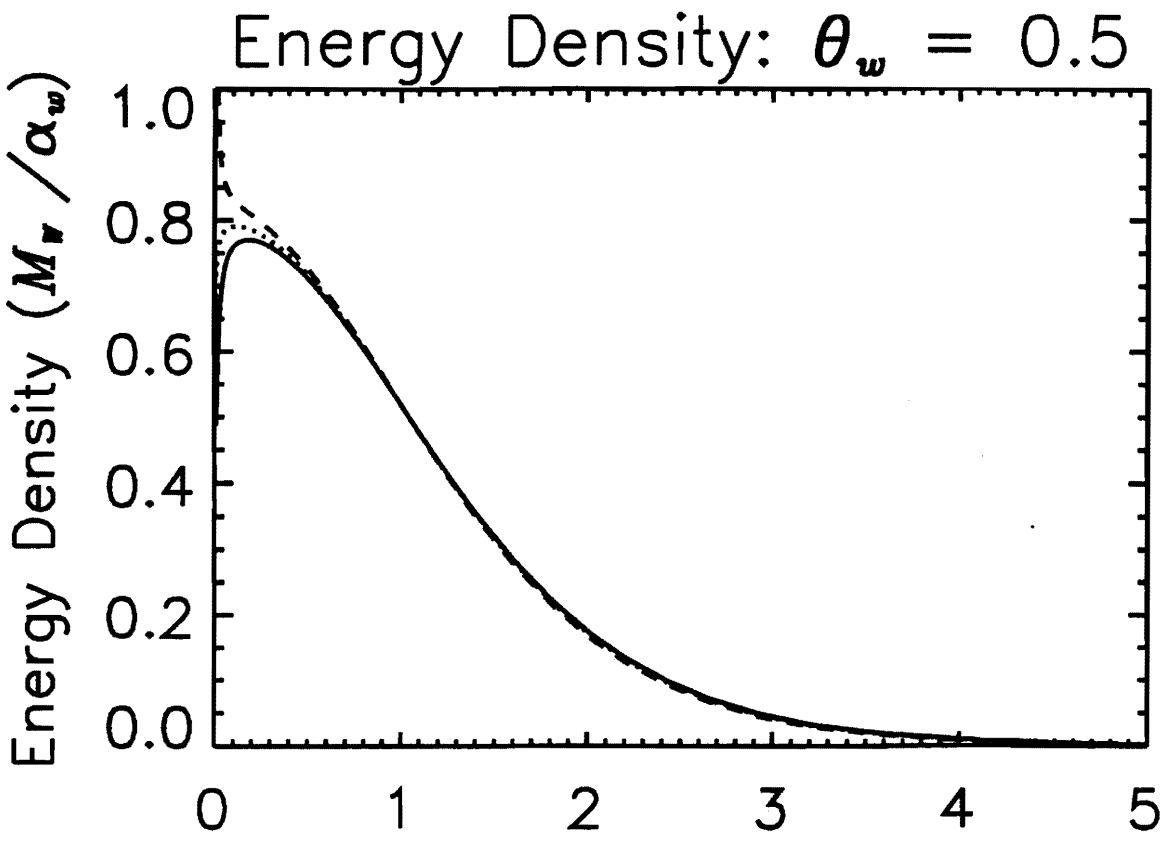
Energy Density: $\theta_w = 0.5$
Energy Density (M_{tt}/α_w)
1.0
0.8
0.6
0.4
0.2
0.0
0
1
2
3
4
5
x

Fig. 15